

This is the accepted manuscript version of the contribution published as:

Schmidt, M., Rohde, F., Braumann, U.-D. (2021):

Visualization and co-registration of correlative microscopy data with the *ImageJ* plug-in
Correlia

Methods Cell Biol. **162** , 353 - 388

The publisher's version is available at:

<http://dx.doi.org/10.1016/bs.mcb.2020.10.001>

Visualisation and co-registration of correlative microscopy data with the *ImageJ* plug-in *Correlia*

Authors:

- Matthias Schmidt (corresponding author)
Department of Isotope Biogeochemistry
Helmholtz Centre for Environmental Research (UFZ)
04318 Leipzig
Germany
E-mail: matthias.schmidt@ufz.de
Orcid ID: 0000-0002-0161-8326
- Florens Rohde
Department of Isotope Biogeochemistry
Helmholtz Centre for Environmental Research (UFZ)
04318 Leipzig
Germany
Orcid ID: 0000-0001-7114-1669
- Ulf-Dietrich Braumann
address 1: Faculty of Engineering, Leipzig University of Applied Sciences (HTWK), Leipzig, Germany
address 2: Fraunhofer Institute for Cell Therapy and Immunology (IZI), Leipzig, Germany
address 3: Institute for Medical Informatics, Statistics and Epidemiology (IMISE), Medical Faculty, Leipzig University, Leipzig, Germany
Orcid ID: 0000-0002-0987-4498

Keywords:

- *Correlia*
- correlative microscopy
- *ImageJ* / *Fiji*
- image registration

- deformable registration
- open source

Abstract

Correlative microscopy experiments require the co-registration of the image data acquired by different micro-analytical techniques. Major challenges are the potentially very different fields-of-view and resolutions as well as the multi-modality of the data. To provide microscopists with an easy-to-use software for two-dimensional image co-registration we have developed *Correlia*, an open-source software based on *ImageJ*¹/*Fiji*², which is fully tailored for the registration of multi-modal microscopy data. It can handle data-sets of in principle arbitrary extent and uses classical approaches, i.e. rigid registration tools or B-spline based deformation models for the correction of both, global and local misalignments, such that a fast registration output is provided. Here we describe some of the basics of *Correlia* focussing on its application: firstly, registration workflows are outlined on artificial data. In the second part these recipes are applied to register correlative data acquired on an algal biofilm and a soil sample.

Introduction

Correlative microscopy is considered the key to understanding complex biological systems on a microscopic scale. One advantage of correlative microscopy lies in the possibility to combine different high-resolution microscopy tools which provide structural details of the specimen (but are chemically-blind) with microanalytical techniques of high chemical- or isotopic sensitivity (but lower spatial resolution) (Caplan et al. 2011; de Boer, Hoogenboom, and Giepmans 2015). Another reason to “go correlative” is that it allows for bridging large scales, i.e. ranging from bird's eye view to ant's view perspective in order to understand the structural and chemical properties. To give an example: one may think of a complex soil sample in which the interplay of plant-roots, soil aggregates, minerals, microbes and small animals like nematodes and earthworms can only be comprehensively understood if it is looked at on different fields-of-view ranging from the centimetre to the sub-micron scale, as the one method helps to localise the microorganisms, while others may provide insight to details concerning the microorganisms and their mutual interplay

1

<https://imagej.net>

2

Fiji is just *ImageJ: Fiji* (Schindelin et al. 2012) is a distribution of *ImageJ* (Rueden et al. 2017), it conveniently bundles many *ImageJ* plug-ins, by this providing a variety of powerful implementations of state-of-the-art methods for scientific image analysis running *ImageJ*, see <https://fiji.sc>

as well as their interaction with the environment. These and many more aspects were already sketched in a topical review entitled “The 2018 correlative microscopy techniques roadmap” by Ando *et al.* (Ando et al. 2018).

The challenges arising from the ambitious endeavour of conducting correlative microscopy and micro analytics on different scales are manifold. A very basic aspect is that protocols for the preparation of the samples have to compromise between a reasonable preservation of the (ultra-)structure of the specimen, while at the same time keeping the chemical composition of the specimen mostly intact. Another point is that imaging workflows have to be thoroughly planned with respect to the destructive properties of each technique such that if technique A and technique B are used in sequence the results of B are not significantly altered by A. Further, some difficulty to relocate one and the same field-of-view in different microscopies might only be overcome by introducing extrinsic marks, e.g. laser marking the sample, or sample holders particularly designed for that purpose. A solution for the latter has been commercialised by Carl Zeiss Microscopy (using the “Shuttle and Find” module of the ATLAS³ software).

Correlative light-electron microscopy (CLEM) is probably the best-known variant of correlative microscopy. However, workflows combining imaging with micro-analytical techniques, e.g. fluorescence in-situ hybridisation combined with nanoSIMS (Musat et al. 2012) or EM and SIMS (Eswara et al. 2019) demonstrate the combinatorial large potential of correlative schemes. For a review on sub-cellular imaging using correlative workflows see (Decelle et al. 2020).

Correlative microscopy experiments require joining the data and deriving additional knowledge from their correlation which usually requires the co-registration of the micrographs onto each other. This in general requires (i) identification of similarities in the moving image (source micrograph) and the target micrographs and can be realised as feature or area-based, (ii) optimisation of a cost function, (iii) selection of a transformation model and (iv) accomplishment of the transformation and resampling of the source micrograph.

There are two basic challenges: firstly, if *arbitrary* microscopic modalities are to be combined, as Decelle *et al.* (Decelle et al. 2020) are outlining, there is no embedded solution available (i.e., in practical research the smallest common denominator often enough are digital micrographs in TIFF⁴ which will have to be imported and registered). Secondly, the workflows may demand further preparation steps (e.g. drying, metallisation

3

<https://www.zeiss.com/microscopy/int/products/microscope-software/atlas.html>

4

<https://www.adobe.io/open/standards/TIFF.html>

etc.) “on the way”, such that various sources for deformations occur in the samples which will require deformable image co-registration. The latter, however, has been considered since several decades in the biomedical field, not only for radiology, but also for histology, as was done e.g. in own work for the 3D reconstruction of tumour tissue based on large histological serial sections (Braumann et al. 2005), (Wentzensen et al. 2007), (Braumann et al. 2007). In fact, correlative microscopy appears to be the most challenging field of application for deformable image co-registration due to the very broad range of types of micrographs.

Ready-to-use software packages for image co-registration tasks are since long existing. One popular is the *Insight Segmentation and Registration Toolkit (Insight Toolkit - ITK⁵)* (McCormick et al. 2014). *ITK* is written in C++⁶ and was wrapped for *Python*⁷, whereas some dedicated multiple wrapping interface called *SimpleITK*⁸ (Yaniv et al. 2019) enables *ITK* usage from C++, *Python*, *R*⁹, *Java*¹⁰, *C#*¹¹, *Lua*¹², *Ruby*¹³ and *Tcl*¹⁴. *ITK* is providing rigid, affine and quite a few deformable registration methods, and is also extendable using plug-ins for registration tasks. One of such plug-ins is *elastix*¹⁵ (Klein et al. 2010) offering implementations of B-splines (with an arbitrary interpolation order), also thin plate splines, and elastic body splines. Since *Elastix*¹⁶ (with capital E) (Tischer 2019) is an *ImageJ/Fiji* wrapper (with some GUI) for *elastix*, it is still not included in *Fiji*, but of course is

5

<https://itk.org>

6

<https://isocpp.org>

7

<https://www.python.org>

8

<http://www.simpleitk.org>

9

<https://www.r-project.org>

10

<https://java.com>

11

<http://csharp.net>

12

<https://www.lua.org>

13

<https://www.ruby-lang.org>

14

<https://www.tcl-lang.org>

15

<https://elastix.lumc.nl> and <https://pypi.org/project/itk-elastix>

16

<https://imagej.net/Elastix>

applicable therein. *bUnwarpJ*¹⁷ (Arganda-Carreras et al. 2006) is implemented in *Java* and is providing cubic B-spline based registration plus some consistency restriction in favour of an invertability of the solution and is included in *Fiji*. *BigWarp*¹⁸ (Bogovic et al. 2016) is also *Java* based and is using thin plate splines. It is also included in *Fiji*, while its functionality lags behind *bUnwarpJ*. *TrakEM2*¹⁹ (Cardona et al. 2012) is also written in *Java*, but offers lots of overall functionality, i.e. manual segmentation, semantic segmentation, skeletonisation, measurements, 3D visualization, image annotation, and also image registration, while the latter is directly based on *bUnwarpJ*. One might have thought that the well-known *OpenCV*²⁰ (an open source computer vision software library written in *C/C++* which can be wrapped for *Python*, *Java*, *Matlab*²¹ and *Octave*²²) does include registration with some non-linear image deformation functionality. However, this is missing so far in *OpenCV*, there are only some affine and projective transformation models implemented yet, so *OpenCV* presently cannot be considered for image co-registration in correlative microscopy.

Amongst the existing software for co-registration of multi-modal image data-sets *easy cell-correlative light to electron microscopy (eC-CLEM)*^{23 24} (Paul-Gilloteaux et al. 2017) is the most prominent solution particularly designed for CLEM. It is a plugin for *Icy*²⁵, a software issued by the Institut Pasteur and France-BioImaging providing a “high-end visual programming framework for seamless development of sophisticated imaging workflows” as it is described in (de Chaumont et al. 2012) (whereas *Icy* in turn can include *ImageJ* within its GUI). *eC-CLEM* has a few unique features, e.g. 3D light microscopies can be co-registered with electron microscopies (2D), it has some integrated image pre-processing and some very intuitive manual/interactive registration using landmarks or reference lines.

17

<https://imagej.net/BUnwarpJ>

18

<https://imagej.net/BigWarp>

19

<https://imagej.net/TrakEM2>

20

<https://opencv.org>

21

<https://www.mathworks.com/products/matlab.html>

22

<https://gnu.org/software/octave>

23

<https://github.com/PerrineGilloteaux/ec-clem>

24

<http://icy.bioimageanalysis.org/plugin/ec-clem>

25

<http://icy.bioimageanalysis.org>

To our knowledge, *eC-CLEM* presently is acknowledged in the correlative microscopy scientific community, it includes a deformable registration mode based on spline interpolation. Together with an additional module, the so called *AutoFinder*²⁶ which does some automatic pre-registration, *eC-CLEM* can be considered very useful for many practical applications, whereas a few open issues remain: it can handle just single image pairs for co-registration, it cannot deal with series (cascades) of image registration steps in an arbitrary sequence (except rigid followed by deformable), it does not include some area-based similarity measure, and it cannot handle visualisations of more than two co-registered images. Some of these aspects, however, are essential for a much broader inclusion of imaging modalities, like nanoSIMS.

Inglada and Giros (Inglada and Giros 2004) adopted several area based similarity measures for multimodal images, including Kolmogorov distance and mutual information (MI; one of the most important similarity measures for multi-modal image registration). Different strategies for the registration of highly multimodal CLEM data are described in the PhD thesis²⁷ of Toledo-Acosta (Toledo Acosta 2018). To the best of our knowledge, there are no tools described yet that provide suitable similarity measures for multimodal images, nonlinear registration methods, and an integrated solution for management and visualisation of multiple correlative images at the same time. Therefore we have developed a new software for exactly that purpose: *Correlia*, an ImageJ plug-in to organise, co-register and visualise multimodal correlative data-sets (Rohde, Braumann, and Schmidt 2020).

Models for image co-registration

Lots of work had been done in the past decades concerning image co-registration (origins thereof go far back to the beginnings of remote sensing), see the famous systematisation done by Gottesfeld Brown (Brown 1992), or some newer review by Zitová and Flusser (Zitová and Flusser 2003), while another extensive review with respect just to the non-linear (deformable, warping) registration methods was given by Sotiras *et al.* (Sotiras, Davatzikos, and Paragios 2013). When designing *Correlia* it had been very clear to us that the software must allow for compensating such mutually non-linear image deformations. According to the categorisation done by Sotiras *et al.*, geometric transformations may

26

<http://icy.bioimageanalysis.org/plugin/ec-clem-autofinder>

27

<https://tel.archives-ouvertes.fr/tel-01868852/document>

either be derived from physical models or from interpolation theory. As was already mentioned above, the use of cubic B-splines was preferred for this work, which obviously are based on interpolation theory. To not consider physical models for *Correlia* so far and to use good old interpolation based ones has a few reasons, (i) as for correlative microscopy in its entirety we have to deal with deformations of a broad variety of causes, it is difficult to estimate physical properties like elasticity. (ii) the computational complexity of geometric transformations derived from physical model is considerably higher than for those derived from interpolation theory, as the former, also referred to as non-parametric registration approaches (see e.g. (Modersitzki 2003), (Fischer and Modersitzki 2004), and (Modersitzki 2009), or own work (Braumann and Kuska 2005), (Braumann and Kuska 2006), (Kuska, Scheibe, and Braumann 2008) and (Scheibe et al.)), are usually based on systems of partial differential equations (PDEs). Compared to, say, spline based approaches PDE-based iterative approaches presently do not allow for interactive applications so far (however, *ITK* already includes some publicly available GPU-adapted implementation of PDE-based image deformable registration methods²⁸, these might be considered in future; also see the *MATLAB*-implementations by Modersitzki *et al.* for *FAIR: Flexible Algorithms for Image Registration*²⁹). (iii) for *Correlia* we were preferring some existing *ImageJ*-related implementation³⁰ of interpolation theory based methods, so the plug-in of choice became *bUnwarpJ*. The cubic B-spline based method implemented in *bUnwarpJ* uses a consistency restriction making sure that the result can be inverted, which guarantees topology preservation, a reasonable property for image registration in general.

Correlia

In this section a quick introduction to the software *Correlia* is given which we hope will enable the reader to use the software for organising, registering and visualising her 2D correlative microscopy data-sets. We will start with a short paragraph on downloading and integrating *Correlia* into an *ImageJ/Fiji* installation. Subsequently, a flow chart for the registration of correlative microscopy data is presented and artificial data-sets are employed to illustrate the different options *Correlia* provides for rigid and deformable image registration.

Installation of the software

Correlia can in principle be installed on any computer with a *Java* 8 (or following versions) runtime environment installed on it and therefore does not depend on a particular operating

28

https://itk.org/Doxygen/html/group__ImageRegistration.html

29

<https://github.com/C4IR/FAIR.m>

30

<https://imagej.net/Registration>

system. We are not exactly sure what the absolute minimum hardware requirements for running *Correlia* are, but so far any modern laptop with at least 2 GB of RAM, a dual core processor and full-HD screen resolution was good enough. However, parts of the programme (in particular the visualisation engine) are already parallelised such that the user will benefit from better machine performance, further parallelisation of the code is planned. On the software side *Correlia* requires a *ImageJ/Fiji* distribution with the plug-in *bUnwarpJ* (Arganda-Carreras et al. 2006) installed. *Fiji* is preferable over *ImageJ* because it is bundled with *bUnwarpJ*. It can be downloaded from <https://imagej.net/Fiji/Downloads>. (The time stamp of the *Fiji* distribution used in this paper is 2019-11-15.) If an *ImageJ* distribution is being used, *bUnwarpJ* has to be installed as well. It can be downloaded from <https://imagej.net/BUnwarpJ>.

Installing *Correlia* is as straight forward as installing any other *Fiji* plug-in and can be done in three steps:

- download the compiled jar-package *correlia.jar* from <http://www.ufz.de/correlia>
- move *ufz-correlia.jar* to the plugins directory of the *ImageJ/Fiji* installation
- restart *ImageJ/Fiji*

Now *Correlia* should be installed and can be run from the *Fiji* menu Plugins → Registration → *Correlia*. *bUnwarpJ* will reside in the same menu, but there is no need to directly invoke it.

Correlia is open source software and can naturally be built from the source code. It is beyond the scope of this chapter to give a full description on how to do that. However, a step by step manual as well as a link to the Git-repository with the source can be found on <http://www.ufz.de/correlia>.

A quick guide to image registration with *Correlia*

Complexity and flexibility make a software package powerful on the one hand but also difficult to learn on the other. The following section will explain the basic aspects of image registration with *Correlia* step by step and will hopefully allow for a smooth and enjoyable start with the software.

In preparation of working with *Correlia*

Fig. 1 displays a workflow for the registration of a correlative data-set. After the acquisition of the image data – micrographs, but also for instance distribution maps of chemical elements and compounds as well as isotopes – it can be imported to *ImageJ/Fiji*. In order to later proceed with *Correlia* it is necessary to calibrate the micrographs properly, in other words to tell the software how many pixels correspond to a physical length unit, e.g. microns. Provided the microscopes are properly calibrated this relation is known (for instance from scale bars) and should be provided to *ImageJ/Fiji* using the function Analyze → Tools → Set Scale. If the respective image format is supported by the Bio-Formats³¹

plug-in (Linkert et al. 2010) the image data can be imported using this plug-in and will immediately be calibrated correctly. Afterwards it is important to save the calibrated micrographs on the hard-drive in TIFF. TIFF is native to *ImageJ/Fiji* and allows for writing the calibration and other useful information to the header. If other image formats are used, e.g. JPEG, PNG, BMP etc., this information will be lost!

Starting a *Correlia* project

Now the data-set is ready to be treated with *Correlia*. For that *Correlia* has to be launched from the *ImageJ/Fiji* menu Plugins → Registration → *Correlia*. Now the user has to select one micrograph in the data-set to become the “canvas” (in *Correlia* referred to as “base image”) onto which the other micrographs should be registered. In general this micrograph should have a large field-of-view and reasonably high resolution and at the same time be rich in features that can serve as intrinsic markers in the registration process.

After that, the graphical user interface (GUI) starts and two windows open: the *Correlia* project viewer and the control frame. The project viewer now only shows the base micrograph, however, after further import of micrographs it will show one particular user-defined representation of the data-set, we will come to that later. Let’s turn to the control frame of the GUI which is displayed in Fig. 2. On the left side a list of all micrographs of the project is displayed, which at the moment only contains the base micrograph. A click on the “+”-button below the list opens the import dialogue such that more micrographs can be imported to the project and are displayed in the list. Selecting a micrograph from the list will display a preview as well as its coordinates relative to the base image on the right side of the main frame. The coordinates allow for a linear (rigid body) transformation; this is translation, rotation and scaling. For rapid pre-alignment the user can set these coordinates manually by typing or clicking on the arrows.

Rigid body registration

After a reasonable manual pre-alignment of the selected micrograph it is ready for rigid body registration. In *Correlia* this can be done

- manually by defining and matching corresponding landmarks in moving image and target or
- automatically by maximising the mutual information of moving image and target.

Fig. 3 illustrates the registration of an artificially blurred test image containing geometrical objects (moving image) onto a non-blurred image containing the same objects but also a chess-board background which is used as base image (target). This test-case relates to the real-life scenario of registering a fluorescence microscopy data with certain fluorescent objects onto electron micrographs which are rich in details.

The top row shows the situation directly after the import of the moving image (left) and a manual pre-alignment (right). For manual registration landmarks were defined at some of the corners of the triangles as well as in the centres of the circles and matched. In order to define landmarks right-click on the previews of the moving image as well as the target image in the *Correlia* control frame. This will open the two micrographs in separate windows with the point-selection tool (build-in feature of *ImageJ*) selected as depicted in Fig. 4A. By point-and-click the landmarks can be defined. After closing the micrograph windows the corresponding landmarks have to be matched by selecting “Align via

features” from the *Correlia* menu “Image”. This will open the “Match features” dialogue and a preview, Fig. 4B. After acceptance of the correspondences the bottom left image of Fig. 3 was obtained.

Admittedly, the registration is far from perfect because only seven points were used for registration and the remaining image content was simply ignored. On top of that, these points were not even well defined in the moving image because of the blurring. A better result was obtained with automatic registration using mutual information, which is shown in the bottom right of Fig. 3. Here the triangles and circles appear to be better aligned because more image content was used for the registration.

In conclusion, in most cases we recommend to do a thorough manual pre-alignment of the moving image followed by the automatic registration. However, in cases of very different image content (e.g. due to very different modality) putting landmarks to features that can be recognised in the moving as well as the target image may be the only way to register.

Deformable registration (de-warping)

In many practical cases rigid body registration of micrographs already meets the requirements of the user if the moving image is free of significant distortions. These, however, cannot always be avoided. On the one hand the sample might deteriorate during a measurement, for instance due to heat generation under the beam of a laser scanning or an electron microscope. On the other hand the correlative microscopy workflow might demand a sample preparation step in between two measurements, which may modify the sample and thereby introduce distortions. Imagine for instance, that in between light and electron microscopy the sample is dehydrated and dried in order to make it vacuum-compatible. This may cause shrinkage or even cracks in the sample which, naturally, result in distortions in the electron micrograph.

In order to register a distorted micrograph properly onto another – ideally distortion-free – modality a non-linear transformation model has to be applied that de-warps the distorted micrograph. Following Sotiras *et al.* we will in the following refer to such a registration step as *deformable registration* (Sotiras, Davatzikos, and Paragios 2013). According to the general workflow for image registration with *Correlia*, displayed in Fig. 1, the user has to make a choice between de-warping the image based on either landmark-matching or areal similarities. The decision structure shown in Fig. 5 shows the different strategies for deformable registration implemented in *Correlia*. A click on the icon “deformable registration” in the main frame (Fig. 2) will change the user interface to deformable transformation mode shown in Fig. 6. Here the user can select from four different strategies to transform the moving image which shall be outlined in the following. An arbitrary number of transformations steps can be cascaded in order to achieve best registration results. Please note that successful registrations can be saved as recipes for future use.

Let’s turn back to Fig. 5 and discuss the options for deformable registration. If the similarities in moving image and target are mainly features, e.g. pin-points or edges, it is advisable to define several features that can be matched by deforming the moving image. In *Correlia* this can be achieved with either “landmarks matching” or using the external plug-in *bUnwarpJ*. The first option has the advantage that the warping can be carried out such that all defined landmarks will be matched exactly. However, the downside is that this may introduce undesired strong distortions in their vicinity. In such cases *bUnwarpJ* is the method of choice: the plug-in allows for compromising between feature alignment

accuracy and the extent of image transformation. The effect of deformable registration by matching landmarks is shown in Fig. 7.

Otherwise, if moving image and target image show common areal similarities - even if these objects are represented by different pixel intensities, e.g. bright in one image and dark in the other - warping methods based on mutual information can be used: Firstly, the “tile matching” approach divides the moving image into overlapping tiles. For each tile the best corresponding area in the target image is determined. The centres of those areas are considered as matching features. This approach works well for large scale deformations. However it cannot be applied to localised distortions as tiles cannot be arbitrary small.

Secondly, the global mutual information (global MI) method computes the similarity on the whole images while iteratively modifying the transformation model. The control points for the transformation can be distributed over the whole image or a specific region of interest. More control points result in a flexible model but also in an increased computational expense. Fig. 8 displays how artificial data is deformable registered with both tile matching and global MI.

Visualisation

A meaningful visualisation of a correlative data-set, naturally, will not display all co-registered micrographs overlaid in one image. Rather, different subsets of micrographs and false-coloured chemical maps are selected in order to visualise particular aspects of the data. For that, the micrographs in a correlative project can either be excluded from visualisation, overlaid fully opaquely or overlaid additively in user-defined false colours. Furthermore it is possible to enhance the contrast of a certain modality.

Two real-life examples

Distribution of phosphorous in an algal biofilm

Rationale:

Phosphorous plays an essential role as fertiliser in agriculture and can lead to eutrophication of waterbodies if present at high levels in wastewater effluents. Microalgal biofilms are known to remove phosphorous from these and therefore have the potential to be used in wastewater treatment plants for this purpose. In their recent study Moreno-Osorio and colleagues employed correlative microscopy to investigate the architecture of *Chlorella* biofilms grown on cotton fabric (Osorio et al. 2019). One aspect of this study was to cultivate the biofilms under phosphorous-rich conditions and investigate whether the algae would store the excess phosphorous either intracellular or within the biofilm matrix.

Here, an algal biofilm from this work shall serve as an example for deformable registration with *Correlia*. For that the structure of the biofilm was investigated by scanning electron microscopy (SEM), and the distribution of phosphorous in the biofilm was measured by energy dispersive X-ray spectroscopy (EDS) in the same SEM. During the EDS

measurement the biofilm degraded under the electron beam such that the phosphorous map contains distortions. We will show how the phosphorous map can be registered onto the SE micrograph, though.

Sample and microscopy equipment

The details of sample growth and preparation for microscopy are given in (Osorio et al. 2019). In brief they are: An algal biofilm of *Chlorella vulgaris* ACUF 809 was cultivated on cotton fabric for 5 days. In preparation of electron microscopy the biofilm was chemically fixed with 4% of paraformaldehyde solution, dehydrated in a graded ethanol series and critical point dried. It was then glued onto standard SEM sample holders (stubs) and sputter-coated with a chromium layer of 20nm thickness.

The analysis was performed with a Zeiss Merlin VP Compact (Carl Zeiss Microscopy, Oberkochen, Germany) field-emission scanning electron microscope coupled with an annular Bruker XFlash Quad 5060F (Bruker Nano GmbH, Berlin, Germany) EDS detector. The electron acceleration energy amounted to 3kV which allowed for obtaining reasonable surface sensitivity but at the same time was sufficiently high to excite the K-alpha line of phosphorous. The beam current was about 250pA.

Methods (for image registration)

Fig. 9 displays SEM data (left) and secondary electron (EDS-SE) image as well as the phosphorous distribution map (EDS-P) measured by EDS (right) side by side. For the registration of the EDS data onto the SEM image it is very helpful that both micrographs, EDS-SE as well as EDS-P, share the same coordinates. In other words, if one of them can be registered onto the SE micrograph this transformation can be applied to the other and will register this one as well. The EDS secondary electron micrograph is of lower resolution than the SEM image. However, in contrast to EDS-P it contains image information similar to the SEM image rendering registration of this modality easier compared to EDS-P.

Following the workflow Fig. 1 the micrographs require proper calibration in preparation of registration with *Correlia*. For that they were opened in *Fiji* and calibrated using “Analyze → Set Scale”. Before calibrating the EDS data both images were put in an image stack³². After calibration, SEM and EDS data were saved in TIFF on the hard-drive.

Subsequently, *Correlia* was started with the scanning electron micrograph used as base image (canvas). Then the stack of EDS-SE and EDS-P was imported such that both will appear as separate images in the *Correlia* project but with coordinates linked. After setting the visualisation-state of EDS-P to “invisible” and a rough manual pre-alignment of EDS-SE onto the scanning electron micrograph the data was ready for automatic rigid

registration based on the mutual information similarity measure. The result is displayed in Fig. 10 in red (EDS-SE) and green (SEM) colouring in order to visualise the differences. Whilst the right-hand side of the micrographs aligns well, it is obvious that in particular areas on the left and in the vicinity of the crack in the biofilm significantly degraded under the electron beam. There, the misalignment is in the order of half of the size of an algal cell. Thus, if the registration were terminated at that point and the rigid transformation of EDS-SE was applied to EDS-P it cannot be decided whether the phosphorous hot spots are inside or outside the algal cells. Therefore further deformable registration steps are required.

The majority of distortions in EDS-SE are areal and extended rather than localised. In such cases the strategy for deformable registration, Fig. 5, suggests to use the tile matching approach. It was clear that the algorithm should be permitted to use the entire deformation scale to de-warp because distortions in the EDS data could neither be classified merely small or large in size. After some trial and error we found that best results were obtained by distributing many small tiles rather than a couple of large ones, therefore the number of tiles (per column/row) was set to six. The result, displayed as red-green difference representation, is shown in Fig. 11 together with a screenshot of the *Correlia* dialogue.

This first de-warping eradicated a number of the extended distortions in EDS-SE, however, further improvement is needed along the crack line through the biofilm on the left side. Since remaining distortions are mostly localised, the strategy (Fig. 5) is to use landmarks based deformable registration either by strict landmark matching or using the external plugin *bUnwarpJ*. We decided to go for the first option and distributed 75 landmarks over the SEM image as well as EDS-SE. The result after matching the landmarks is displayed in Fig. 12. The accuracy of the registration is, excepting a few bacteria and filaments of exopolymeric substances, better than one tenth of the size of an algal cell and therefore suffices for answering the initial question whether phosphorous deposits are in- or outside the algal cells. Switching the visualisation state of EDS-SE to “invisible” and that of EDS-P to “enhanced” in red colour yields Fig. 13. Now it is clear that the microalgae store excess phosphorous inside the cells rather than in the biofilm which is in line with the time-of-flight secondary ion mass spectroscopy data published in (Osorio et al. 2019).

Alternatives and troubleshooting

There is no such thing as the “golden trail” to perfect registration, and a similar result could have been obtained using other registration possibilities implemented in *Correlia*. For instance, rigid registration by defining and matching corresponding landmarks in the target and the moving image will result in a reasonable prealignment as well. Also, as first elastic registration step one could have used the global mutual information algorithm instead of tile matching. This, as said earlier, is recommended if the areal distortions in the moving

image can be regarded localised rather than extended. An alternative for the second deformable registration step, in which we went for strict matching of landmarks, could be using the *bUnwarpJ*-based deformable registration approach in *Correlia*. The difference is that instead of matching landmarks absolutely perfectly (no matter if that requires the introduction of new areal distortions in the moving image, cp. Fig. 7A and B) *bUnwarpJ* un-warps the moving image with respect to matching of landmarks on the one hand but also keeping the deformation-introduced distortions small on the other. The user may put more weight for compromising onto either landmarks or areal similarities, cp. Fig. 7B, C and D.

Summary

This example showed how interlinked micrographs which share their coordinates because they were acquired together in the same experiment (here EDS-SE and EDS-P) can be registered onto another micrograph (SEM) by merely registering the most suitable modality (here EDS-SE) and applying the transformation model to the other (EDS-P). This piggyback approach is suitable for many microanalytical techniques producing a number of for instance chemical distribution maps at the same time. Furthermore the example illustrated how distortions in the moving image can be un-warped in two subsequent deformable registration steps using *Correlia*.

Microscopic analysis of a soil sample - An image registration workflow

Rationale:

Studying the interplay of plant roots, mineral particles, organic matter and microbes in soil is a complicated matter. It requires a sample preparation that allows for structural analysis from the centimetre down to the sub-micrometre scale with respect to root geometry, pores etc. At the same time the chemical composition of the soil sample must not be disturbed significantly such that micro-analytical techniques can be employed to measure chemical gradients and matter fluxes (of for instance carbon or nitrogen) in the vicinity of a root. Recently Schlüter, Eickhorst and Mueller (Schlüter, Eickhorst, and Mueller 2019) published a novel protocol for correlative imaging of soil. It combines computer tomography for the acquisition of a 3D-tomogram of the soil core with 2D microscopy and micro-analytics measured on a plane dissecting the core physically by sawing and polishing.

Here, we demonstrate how *Correlia* can be used for the registration of several 2D data acquired on a similar sample which was prepared and provided by one of the authors of the referenced study (S. Schlüter). The example shows *Correlia*'s capability to handle medium-size data-sets comprising micrographs and maps of various modalities acquired on fields-of-view that differ by about two orders of magnitude.

Sample and microscopy equipment:

The sample is soil that was chemically fixed, dehydrated, embedded in epoxy-resin, sawn with a diamond saw and polished. The structural analysis of the so-prepared sample was carried out by

- a Sensofar SNeox 3D optical profilometer, Sensofar Metrology, Terrassa, Spain
- a Zeiss Orion NanoFab scanning helium-ion microscope, Zeiss Peabody, MA, USA.

The atomic composition of the sample was checked with a

- Bruker QUANTAX FlatQUAD energy-dispersive X-ray spectrometer, Bruker Nanoanalytics, Berlin, Germany mounted in a
- Zeiss Merlin VP Compact scanning electron microscope, Carl Zeiss Microscopy, Oberkochen, Germany.

Chemical micro-analysis was performed with

- an IONTOF ToF.SIMS5 time-of-flight secondary ion mass spectrometer, IONTOF, Münster, Germany.

Methods:

We present a workflow for the correlative analysis of the soil sample where acquisition and registration of microscopic data are closely entangled. Basically, it consists of the following steps:

1. acquisition of an overview map, in the following referred to as *treasure map*, by stitching many fields-of-view acquired by optical microscopy at low magnification
2. identification of a region of interest (ROI) which contains a plant root
3. start a new *Correlia* project with the part of the treasure map that contains the ROI which serves as canvas for the registration of subsequently acquired micrographs
4. structural analysis of the vicinity of the root by high-resolution helium-ion microscopy
5. registration of the helium-ion microscopy (HIM) data onto treasure map
6. topography measurement by optical profilometry at high-resolution
7. registration of the topography map onto the HIM image
8. chemical micro-analysis by time-of-flight secondary ion-mass spectrometry (ToF-SIMS)

9. rigid and deformable registration of the ToF-SIMS data onto HIM image
10. metallisation (sputter-coating) of the sample with Au/Pd (80:20) in preparation of energy dispersive X-ray spectroscopy (EDS)
11. analysis of the atomic composition of the minerals in the vicinity of the root by EDS

M1, M2 - Acquisition of a treasure map and identification of areas of interest

Experimentally the correlative workflow has to be planned carefully with respect to the effects of the different micro-analytical techniques on the soil sample. It is also important that such a workflow contains the acquisition of a treasure map to have a reference for navigation on the sample which allows for conveniently finding back regions of interest (ROIs) in the different microscopes. A treasure map can in principle be obtained by any microscope capable of measuring at sufficiently large field-of-view with sufficiently large depth of focus at medium resolution. It is important that the treasure map contains at least some structural information of all parts of the sample. (Fluorescence microscopy for instance would not be a good choice since non-fluorescent areas will appear dark and thus are free of information.) This ensures that at least in principle any object of choice appearing in the micrographs and chemical maps acquired subsequently can be used to register these onto the treasure map.

Having that in mind the embedded soil sample was put under the optical profilometer which in principle is an optical microscope suitable to measure samples with a surface topography. For that it uses focus-variation to acquire a z-stack of planes of which only certain areas are in focus. From this z-stack an algorithm known as focus stacking calculates an all-focussed micrograph as well as a height map of the surface. Furthermore the instrument allows for stitching together many fields-of-view such that an almost arbitrarily large map can be obtained.

In this case a 10× objective was used and 6×6 fields-of-view were stitched together resulting in a map $8.1 \times 7.3 \text{ mm}^2$ at an isotropic pixel-size of about $1.3 \mu\text{m}$. On the treasure map an area of interest containing a plant root was identified as indicated on the left of Fig. 15. In principle the correctly calibrated treasure map could serve as canvas (base image) for the *Correlia* project. However, none of the following analyses was to be conducted outside the ROI. Thus it appears to be more convenient on the one hand, but also memory-saving on the other to start the *Correlia* project with a highly resolved map of the ROI.

With that in mind, a second, more detailed bright-field micrograph of the ROI was acquired with the optical profilometer using a 50× objective and stitching 5×6 fields of view such that an area of $1600 \times 1450 \mu\text{m}^2$ resolved at $6253 \times 5632 \text{ pixels}^2$ was obtained (inset of Fig. 15, left) .

M3 - Start a new *Correlia* project

In order to start a new *Correlia* project with the optical profilometer micrograph of the ROI as canvas (base image) correct calibration of the same has to be ensured. For that the micrograph was opened with *Fiji* and using Analyze → Set Scale it was checked that 1µm equals 3.88pixels. Then *Correlia* was started from the “Plugins” menu and the calibrated micrograph was used as canvas (base image). At this point it is good practice to title the project properly and leave some information about the sample and the purpose of the study. This can be done by calling “Project → Project Properties” from the *Correlia* main frame.

M4, M5 - Scanning helium ion microscopy

The resolution of optical microscopy is restricted to about 0.3µm due to the Abbe limit. Higher lateral resolution can for instance be obtained with either SEM or HIM. For the non-conductive soil-sample HIM appeared to be the more suitable technique because it has the advantage of larger depth-of-field compared to SEM (Ward, Notte, and Economou 2006) and the possibility of efficient charge compensation. The electron flood gun of the HIM allows for compensating the implanted positive charges of the He⁺ ions after each scanned line and in turn does not require carbon-coating or metallisation of the sample which normally has to be done prior to SEM analysis³³.

The sample was subjected to HIM analysis using an ion-landing energy of 25kV and secondary electron detection. With the aid of the treasure map the area of interest was quickly found back and an overview image as well as a micrograph revealing details of the surrounding of the root were acquired. The HIM overview was manually registered onto the bright-field micrograph matching landmarks. The result is shown on the right side of Fig. 15 with the root encircled. It is obvious that the modalities are too different to be automatically registered: Whilst HIM mainly shows a topography contrast with a probing depth of only a couple of nanometers below the surface, contrast in the bright-field treasure map is gained from the reflection of light at the surface, a process happening on length scales in the order of at least some wavelengths of the exciting light.

Fig. 16 depicts the vicinity of the root as shown by the different micro-analytical techniques. In sub-figure B the high-resolution HIM image showing the plant-cells is auto-registered onto the HIM overview. Sub-figure C serves to show the quality of the registration of the HIM image (here false-coloured in blue) onto the bright-field image.

³³Carl Zeiss Microscopy, White papers: Zeiss Orion Plus (2008) and Zeiss Orion NanoFab (2016), <https://www.zeiss.com/microscopy/int/products/multiple-ion-beam/orion-nanofab-for-materials.html>.

M6, M7 - Measurement of the topography in the vicinity of the plant root

In order to conclude on the quality of the sample preparation, e.g. infiltration of the resin, sawing and polishing, the topography was measured with the optical profilometer in the vicinity to the plant-root. For that a confocal z-stack was acquired using a 100× objective and blue excitation from a light emitting diode. Lateral as well as depth resolution of the obtained topography map are better than 0.5µm. Subsequently the false-coloured map – bottom (blue) to top (red) equals 17µm – was imported to the project and rigidly registered onto the HIM image using the automatic algorithm. Since in both micrographs the plant-cells in the root are easily recognised and on top of that the micrographs are almost distortion-free a high-quality overlay was obtained, Fig. 16D. Please note that registering the topography map onto HIM at the same time registers it onto the treasure map because HIM and treasure map had previously been registered.

M8, M9 – Time-of-flight secondary ion mass spectrometry

Up to this point only structural information but no chemical information about the sample was obtained. In order to gain some insight into the chemical composition of the sample ToF-SIMS was employed to measure molecular ion maps. For that, the sample was scanned with a beam of bismuth ion clusters (Bi_3^+) (Touboul et al. 2005) allowing for imaging in negative ion extraction mode. Since ToF-SIMS acquires a full ion-detection spectrum for each pixel, distribution maps for several negatively charge ions are obtained at the same time. For demonstrating the process of registration of the ToF-SIMS data we will merely focus on the $^{12}\text{C}^{14}\text{N}^-$ signal (for simplicity in the following referred to as CN^-), which serves as a marker for biomass (Benettoni et al. 2019) and the total ion count (TIC) which provides structural information similar to HIM. It is important to mention that a ToF-SIMS measurement is performed such that the exciting beam hits the sample under an angle of 45° and that the secondary ions are extracted perpendicularly to the surface. This geometry naturally introduces distortions in the obtained maps which will have to be taken into consideration for image registration.

In Fig. 17 HIM and ToF-SIMS data (TIC and CN^-) acquired on the root are displayed next to each other. In step 1 HIM and TIC were rigidly auto-registered onto each other. The false-colour overlay of HIM (green) and TIC (red) shows a reasonable alignment of both maps. TIC and CN^- maps were acquired in the same measurement and thus share the same coordinates which, as in the previous example, allows for linking both and in turn get CN^- registered onto HIM as well (step 2). The overlay of HIM (green) and CN^- (red) suggests de-warping. The distortions in CN^- are neither purely areal nor can they be considered localised. Therefore, two approaches were tried out: in 3a) deformable registration using global MI in a ROI around the root with 4×4 control points³⁴ was used, however, only

³⁴ In the software referred to as “deformation handles”.

minor improvements were achieved. More successful was the usage of *bUnwarpJ*, step 3b), by distributing about a dozen landmarks onto the walls of the plant-cells and matching them. Fig. 16F shows the heat map of the ToF-SIMS CN⁻ map in the context of the other modalities. In conclusion it can be said that, as expected, CN⁻ is a marker for biomass and is therefore mainly measured in the root.

M10, M11 – Chemical analysis of mineral particles by energy- dispersive X-ray spectroscopy

In order to get deeper insight into the mineralogy of the vicinity of the root, which would be an important parameter for understanding (bio-)geochemical processes occurring in the rhizosphere, element distribution maps were measured by EDS. In preparation of these experiments the sample had to be sputter-coated with chromium³⁵ to obtain a conductive surface. With the aid of both, bright-field treasure map and HIM, it was easy to find back the ROI in the SEM. Similar to the procedure shown in the example of the algal biofilm the secondary electron signal EDS-SE was used to register the EDS-maps onto the HIM image. For that rigid registration was absolutely sufficient.

Regarding the image registration functionality of *Correlia* we could at this point finish this example showing an overlay of the EDS data with another modality. However, the EDS maps are suitable to demonstrate another useful functionality of *Correlia*. Fig. 18 shows the element distribution maps of sodium, magnesium, aluminium, silicon, potassium and iron which are typical components of soil minerals. Looking merely at the chemical elements does not reveal the type of minerals present in the sample, though. Silicon, for instance, is present in quartz (SiO₂) and feldspars (aluminium silicates) as well. In order to derive new knowledge from correlative data *Correlia* has a function to “product correlate” images. For that, the image intensity $I_d(x,y)$ in the derived image at each data point (x,y) is calculated from the normalised³⁶ intensities of the n correlated images at the same point $I_i(x,y)$:

$$I_d(x, y) = \sqrt[n]{\prod_{i=1}^n I_i(x, y)}$$

We applied product correlation to the element maps and derived maps of Na-feldspar (Na, Al, Si), K-feldspar (K, Al, Si) and an magnesium, aluminium and iron containing mineral which is likely to be pleonast. The residual silicon signal that does not originate from the

35

Chromium was chosen as its characteristic X-ray lines do not interfere with those of the chemical elements of interest in this study, namely C, Na, Mg, Al, Si, P, K and Fe.

36

Normalisation is done such that the lowest value (dark) is considered 0 and the point of highest intensity is set to 1.

feldspars very likely originates from quartz minerals. Fig. 19 shows an overlay of these mineral maps together and the EDS-C signal (green, mainly indicating the epoxy resin) with the HIM image.

Summary

In this example we demonstrated how *Correlia* can be used to organise and register medium-sized correlative data-sets. In particular we showed that in principle it is possible to register any micrograph in the *Correlia* project onto any other. We also used the different options available to the user to visualise the correlative data in meaningful ways. Finally we showed how additional knowledge can be obtained from correctly registered correlative data using the product correlation function of *Correlia*.

Summary and Conclusions

In this chapter we demonstrated how the new software *Correlia* can be used to organise, co-register and visualise 2D multi-modal correlative microscopy data-sets interactively, in particular using semi-automated procedures. *Correlia* organises the image data in projects which can be extended and annotated at any time in the workflow by the user(s). This may be beneficial for microscopists working together, since sharing such a project amongst each other is not mere exchange of data but also of context and derived knowledge.

Using artificial data we outlined general workflows for registration of micrographs and micro-analytical maps with *Correlia*. These typically comprise manual or automatic rigid (pre-)registration followed by one or many cascaded deformable registration steps. The workflows were tested on real-life data-sets acquired on an algal biofilm and a soil sample. In both examples, there were subsets of micrographs originating from the same measurement (e.g. a stack of chemical maps) and thus sharing the same coordinates. For such cases it proved useful to register one of the micrographs and use the build-in option to translate the transformation model to the other micrographs in order to register them as well. The examples we used suggest that warped micrographs should be deformably registered twice to align properly with the target: In the first step areal distortions are treated using either the “global MI” or “tile-matching” algorithms. In the second step manually set landmarks in source and target are matched. Moreover the image registrations performed on the data acquired on the soil sample showed that the target micrograph for registration does not necessarily have to be the same for all modalities but a registered micrograph can serve as a target for another modality. Therefore, *Correlia* allows for registering any micrograph in the project onto any other.

Embracing the idea of gaining additional knowledge by correlating data rather than looking at single measurements *Correlia* offers a function to product-correlate two or more previously registered micrographs. The functionality is particularly useful for chemical

maps since the analytical capabilities of different techniques can be combined. To illustrate this we used product-correlation to determine different types of minerals in the vicinity of a plant root from elemental maps obtained from energy-dispersive X-ray spectroscopy measurements.

Having registered all micrographs in a data-set the microscopist wants to visualise her work in a meaningful way. For that *Correlia* allows for choosing false colours, switching on and off micrographs and enhancing their contrast. In combination with the full power of image-processing inherited from the *Fiji/ImageJ* environment correlative data-sets can be turned into scientific knowledge and visual art at the same time.

Acknowledgements

The authors are thankful to Jairo Hernán Moreno Osorio and Steffen Schlüter for providing the microalgal biofilm and the soil sample, respectively. We furthermore thank Hryhoriy Stryhanyuk for helpful discussions and for the acquisition of chemical maps on the soil sample with time-of-flight secondary ion mass-spectrometry. The authors are grateful for using the laboratories and experimental facilities at *ProVIS – Centre for Chemical Microscopy* at the Helmholtz Centre for Environmental Research, Leipzig, which is supported by the European Regional Development Fund (ERDF, operational programme for Saxony), and the Helmholtz Association.

List of Figures

Figure 1: Workflow for the registration of correlative micrographs using Correlia.

Figure 2: *Correlia*'s graphical user interface.

Figure 3: Illustration of the two possible ways for rigid body registration in Correlia. The moving image only contains some geometrical objects (red) which are supposed to align with the black objects on the chess board (target image). On the one hand corresponding landmarks can be defined in both, moving image and target which will be matched. On the other hand automatic registration using a mutual information approach is possible after a manual pre-alignment.

Figure 4: Rigid body registration using landmarks. A) At least three landmarks are defined in moving image and target. B) Afterwards, corresponding features have to be matched. In the "Match Features" dialogue the user can either set the correspondences manually or ask the software to guess. The feature correspondences are then displayed with light blue lines in the viewer. The user acceptance of the correspondences will calculate the coordinates x and y as well as rotation and scale that will register the moving image onto the target.

Figure 5: Rigid body registration cannot lead to a proper image alignment if distortions are present in the moving image. However, this can still be achieved by subsequently applying one or more of the deformable registration algorithms implemented in *Correlia* to de-warp the moving image. This flow chart shall help to select the most suitable one for the given registration problem.

Figure 6: *Correlia*'s graphical user interface for deformable image registration. Several transformation steps can be cascaded and are listed on the left (here: "tile matching" followed by "landmarks"). The chess-board image on the right displays the transformation field. The parameters for the selected transformation are shown below.

Figure 7: If a distorted moving image contains feature-points that have correspondences in the target, landmarks can be defined in both and "forced" to align. Correlia supports pure landmark-matching but also uses the external plug-in *bUnwarpJ*. The latter offers the possibility to transform the moving image in different ways by putting certain weight on image content (img) and landmarks (lm).

Figure 8: Registration of a moving image with artificial areal distortions onto a non-distorted but Gaussian-blurred target. After rigid pre-registration the moving image was warped to align with the target. For that tile matching with 4 and 25 tiles as well as global mutual information using 4 and 16 deformation handles were used, respectively.

Figure 9: Investigation of the distribution of phosphorous in a biofilm of *Chlorella sp.* microalgae. A scanning electron micrograph (SEM, left) shall be overlaid with energy-dispersive X-ray spectroscopy maps (SEM-EDS, right). For that the secondary electron micrograph of the SEM-EDS data has to be registered onto the SEM image. Once that is done the same transformation can be applied to the phosphorous map which then will be registered as well.

Figure 10: Rigid registration: Difference representation of the result of automatic rigid registration of SEM-EDS-SE (red) onto the SEM image (green) taken on the algal biofilm displayed in Fig. 9. Whilst the right side of the overlay aligns well, distortions along the crack on the left of the overlay are obvious and call for further deformable transformation.

Figure 11: Deformable registration 1 (tile matching): Difference image of SEM (green) overlaid with SEM-EDS secondary electron micrograph (red) of the algal biofilm shown in Fig. 9 and 10 after the first deformable registration using the tile matching approach. The tile matching was carried out with 6x6 tiles distributed over the source micrograph allowing for full deformation scale. In particular on the left side of the image a significant improvement of the registration was achieved.

Figure 12: Deformable registration 2 (landmarks matching): After rigid pre-alignment (Fig. 10) and a deformable registration step (tile matching, Fig. 11) a final deformable registration step using landmarks matching is employed to properly register SEM image (green) and SEM-EDS secondary electron micrograph (red) acquired on a *Chlorella sp.* biofilm. In the upper part of the figure the distribution of landmarks in both micrographs is shown. The lower part shows the registration result after matching them.

Figure 13: Application of the transformation model obtained by deformable registration of the SEM-EDS secondary electron micrograph onto the SEM image measured on the algal biofilm of *Chlorella sp.* microalgae (Fig. 12) to SEM-EDS phosphorous distribution map (shown in red). This overlay with the SEM image shows that the microalgae store excess phosphorous inside the cells rather than in the matrix of exopolymeric substances in the biofilm.

Figure 14: Workflow illustrating the sequence of microscopic analyses of the soil sample and at the same time the sequence of image registration applied to the so obtained correlative microscopy data.

Figure 15: Treasure maps acquired on the soil sample. A) Stitched bright field image of the sample with the region of interest indicated and magnified. A root is found and encircled in white. B) The bright-field image of the region of interest serving as canvas (base image) for the Correlia project is overlaid with a helium-ion micrograph.

Figure 16: Organisation and visualisation of different modalities: A) Bright-field micrograph of the root found in the soil sample acquired with the optical profilometer. B) The same field-of-view imaged with the helium-ion microscope. A close-up of the root was taken at higher resolution and registered (rigid) onto the overview image. C) Overlay of bright-field image and HIM (false coloured in blue). D) Topography map measured with the optical profilometer using a 100x air-objective registered onto the HIM image. The difference in height, from dark blue to red, amounts to 17 microns. E) Composite of chemical maps acquired by SEM-EDX registered onto the bright-field micrograph. F) Intensity map of CN⁻ ions measured by ToF-SIMS deformed and registered onto the helium ion micrograph.

Figure 17: Registration of ToF-SIMS data onto HIM: 1) The ion count (TIC) obtained from ToF-SIMS is very similar to the helium-ion micrograph. After rigid registration the difference image with HIM in green and ToF-SIMS in red shows a good correlation. 2) Applying this transformation model to the CN⁻ ion distribution map. Deformable registration can locally improve the quality of the registration as shown by the results of global mutual information (3a) and bUnwarpJ (3b).

Figure 18: Correlation of SEM-EDS maps: If element distribution maps measured by SEM-EDS are pixelwise multiplied additional chemical information can be gained. Here for instance, different aluminium silicates can be grouped into different types of feldspar with aid of the Na and K maps. Furthermore the correlation of Mg, Al and Fe maps hints to the presence of the mineral pleonast in the sample. The composite image of the gained mineralogical maps is shown in Fig. 18.

Figure 19: Overlay of the helium-ion micrograph and mineralogical maps gained from the correlation of SEM-EDS chemical maps. Plant-cells in the root and pores are filled with resin (green, measured as carbon distribution map by SEM-EDS). The minerals in the vicinity of the root are quartz and different feldspar minerals.

References

- Ando, Toshio, Satya Prathyusha Bhamidimarri, Niklas Brending, H. Colin-York, Lucy Collinson, Niels De Jonge, P. J. de Pablo, Elke Debroye, Christian Eggeling, Christian Franck, Marco Fritzsche, Hans Gerritsen, Ben N. G. Giepmans, Kay Grunewald, Johan Hofkens, Jacob P. Hoogenboom, Kris P. F. Janssen, Rainer Kaufmann, Judith Klumperman, Nyoman Kurniawan, Jana Kusch, Nalan Liv, Viha Parekh, Diana B. Peckys, Florian Rehfeldt, David C. Reutens, Maarten B. J. Roeffaers, Tim Salditt, Iwan A. T. Schaap, Ulrich S. Schwarz, Paul Verkade, Michael W. Vogel, Richard Wagner, Mathias Winterhalter, Haifeng Yuan, and Giovanni Zifarelli. 2018. 'The 2018 correlative microscopy techniques roadmap', *Journal of Physics D: Applied Physics*, 51: 443001.
- Arganda-Carreras, Ignacio, Carlos O. S. Sorzano, Roberto Marabini, José María Carazo, Carlos Ortiz-de-Solorzano, and Jan Kybic. 2006. "Consistent and Elastic Registration of Histological Sections Using Vector-Spline Regularization." In, 85-95. Berlin, Heidelberg: Springer Berlin Heidelberg.
- Benettoni, Pietro, Hryhoriy Stryhanyuk, Stephan Wagner, Felix Kollmer, Jairo H. Moreno Osorio, Matthias Schmidt, Thorsten Reemtsma, and Hans-Hermann Richnow. 2019. 'Identification of nanoparticles and their localization in algal biofilm by 3D-imaging secondary ion mass spectrometry', *Journal of Analytical Atomic Spectrometry*, 34: 1098-108.
- Bogovic, J. A., P. Hanslovsky, A. Wong, and S. Saalfeld. 2016. "Robust registration of calcium images by learned contrast synthesis." In *2016 IEEE 13th International Symposium on Biomedical Imaging (ISBI)*, 1123-26.
- Braumann, U. D., N. Scherf, J. Eickenkel, L. C. Horn, N. Wentzensen, M. Loeffler, and J. P. Kuska. 2007. 'Large Histological Serial Sections for Computational Tissue Volume Reconstruction', *Methods Inf Med*, 46: 614-22.
- Braumann, U., and J. Kuska. 2005. "Influence of the boundary conditions on the result of non-linear image registration." In *IEEE International Conference on Image Processing 2005*, I-1129.
- . 2006. "A New Equation for Nonlinear Image Registration with Control over the Vortex Structure in the Displacement Field." In *2006 International Conference on Image Processing*, 329-32.
- Braumann, U., J. Kuska, J. Eickenkel, L. Horn, M. Loeffler, and M. Hockel. 2005. 'Three-dimensional reconstruction and quantification of cervical carcinoma invasion fronts from histological serial sections', *IEEE Transactions on Medical Imaging*, 24: 1286-307.
- Brown, Lisa Gottesfeld. 1992. 'A survey of image registration techniques', *ACM Comput. Surv.*, 24: 325–76.
- Caplan, Jeffrey, Marc Niethammer, Russell M. Taylor, and Kirk J. Czymmek. 2011. 'The power of correlative microscopy: multi-modal, multi-scale, multi-dimensional', *Current Opinion in Structural Biology*, 21: 686-93.
- Cardona, Albert, Stephan Saalfeld, Johannes Schindelin, Ignacio Arganda-Carreras, Stephan Preibisch, Mark Longair, Pavel Tomancak, Volker Hartenstein, and

- Rodney J. Douglas. 2012. 'TrakEM2 Software for Neural Circuit Reconstruction', *PLOS ONE*, 7: e38011.
- de Boer, Pascal, Jacob P. Hoogenboom, and Ben N. G. Giepmans. 2015. 'Correlated light and electron microscopy: ultrastructure lights up!', *Nature Methods*, 12: 503-13.
- de Chaumont, Fabrice, Stéphane Dallongeville, Nicolas Chenouard, Nicolas Hervé, Sorin Pop, Thomas Provoost, Vannary Meas-Yedid, Praveen Pankajakshan, Timothée Lecomte, Yoann Le Montagner, Thibault Lagache, Alexandre Dufour, and Jean-Christophe Olivo-Marin. 2012. 'Icy: an open bioimage informatics platform for extended reproducible research', *Nature Methods*, 9: 690-96.
- Decelle, Johan, Giulia Veronesi, Benoit Gallet, Hryhoriy Stryhanyuk, Pietro Benettoni, Matthias Schmidt, Rémi Tucoulou, Melissa Passarelli, Sylvain Bohic, Peta Clode, and Niculina Musat. 2020. 'Subcellular Chemical Imaging: New Avenues in Cell Biology', *Trends in Cell Biology*, 30: 173-88.
- Eswara, S., A. Pshenova, L. Yedra, Q. H. Hoang, J. Lovric, P. Philipp, and T. Wirtz. 2019. 'Correlative microscopy combining transmission electron microscopy and secondary ion mass spectrometry: A general review on the state-of-the-art, recent developments, and prospects', *Applied Physics Reviews*, 6: 021312.
- Fischer, Bernd, and Jan Modersitzki. 2004. 'A unified approach to fast image registration and a new curvature based registration technique', *Linear Algebra and its Applications*, 380: 107-24.
- Inglada, J., and A. Giros. 2004. 'On the possibility of automatic multisensor image registration', *IEEE Transactions on Geoscience and Remote Sensing*, 42: 2104-20.
- Klein, S., M. Staring, K. Murphy, M. A. Viergever, and J. P. W. Pluim. 2010. 'elastix: A Toolbox for Intensity-Based Medical Image Registration', *IEEE Transactions on Medical Imaging*, 29: 196-205.
- Kuska, J., P. Scheibe, and U. Braumann. 2008. "Fast fluid extensions for image registration algorithms." In *2008 15th IEEE International Conference on Image Processing*, 2408-11.
- Linkert, Melissa, Curtis T. Rueden, Chris Allan, Jean-Marie Burel, Will Moore, Andrew Patterson, Brian Loranger, Josh Moore, Carlos Neves, Donald MacDonald, Aleksandra Tarkowska, Caitlin Sticco, Emma Hill, Mike Rossner, Kevin W. Eliceiri, and Jason R. Swedlow. 2010. 'Metadata matters: access to image data in the real world', *Journal of Cell Biology*, 189: 777-82.
- McCormick, Matthew, Xiaoxiao Liu, Luis Ibanez, Julien Jomier, and Charles Marion. 2014. 'ITK: enabling reproducible research and open science', *Frontiers in Neuroinformatics*, 8.
- Modersitzki, Jan. 2003. *Numerical Methods for Image Registration* (Oxford University Press).
- . 2009. *FAIR: Flexible Algorithms for Image Registration - Software and Apps* (SIAM - Society for Industrial and Applied Mathematics).
- Musat, Niculina, Rachel Foster, Tomas Vagner, Birgit Adam, and Marcel M. M. Kuypers. 2012. 'Detecting metabolic activities in single cells, with emphasis on nanoSIMS', *FEMS Microbiology Reviews*, 36: 486-511.
- Osorio, Jairo H Moreno, Pietro Benettoni, Matthias Schmidt, Hryhoriy Stryhanyuk, Mechthild Schmitt-Jansen, Gabriele Pinto, Antonino Pollio, Luigi Frunzo, Piet N L Lens, Hans H Richnow, Giovanni Esposito, and Niculina Musat. 2019.

- 'Investigation of architecture development and phosphate distribution in Chlorella biofilm by complementary microscopy techniques', *FEMS Microbiology Ecology*, 95.
- Paul-Gilloteaux, Perrine, Xavier Heiligenstein, Martin Belle, Marie-Charlotte Domart, Banafshe Larijani, Lucy Collinson, Graça Raposo, and Jean Salamero. 2017. 'eC-CLEM: flexible multidimensional registration software for correlative microscopies', *Nature Methods*, 14: 102-03.
- Rohde, Florens, Ulf-Dietrich Braumann, and Matthias Schmidt. 2020. 'Correlia: an ImageJ plug-in to co-register and visualise multimodal correlative micrographs', *Journal of Microscopy*, 280: 3-11.
- Rueden, Curtis T., Johannes Schindelin, Mark C. Hiner, Barry E. DeZonia, Alison E. Walter, Ellen T. Arena, and Kevin W. Eliceiri. 2017. 'ImageJ2: ImageJ for the next generation of scientific image data', *BMC Bioinformatics*, 18: 529.
- Scheibe, Patrick, Tino Wetzig, Jens-Peter Kuska, Markus Löffler, Jan C. Simon, Uwe Paasch, and Ulf-Dietrich Braumann. '3D-Reconstruction of Basal Cell Carcinoma, A Proof-of-Principle Study.' in B. Fischer, Dawant B.M. and Lorenz C. (eds.), *Biomedical Image Registration* (Springer: Berlin, Heidelberg).
- Schindelin, Johannes, Ignacio Arganda-Carreras, Erwin Frise, Verena Kaynig, Mark Longair, Tobias Pietzsch, Stephan Preibisch, Curtis Rueden, Stephan Saalfeld, Benjamin Schmid, Jean-Yves Tinevez, Daniel James White, Volker Hartenstein, Kevin Eliceiri, Pavel Tomancak, and Albert Cardona. 2012. 'Fiji: an open-source platform for biological-image analysis', *Nature Methods*, 9: 676-82.
- Schlüter, Steffen, Thilo Eickhorst, and Carsten W. Mueller. 2019. 'Correlative Imaging Reveals Holistic View of Soil Microenvironments', *Environmental Science & Technology*, 53: 829-37.
- Sotiras, A., C. Davatzikos, and N. Paragios. 2013. 'Deformable Medical Image Registration: A Survey', *IEEE Transactions on Medical Imaging*, 32: 1153-90.
- Tischer, Christian. 2019. 'ElastixWrapper: Fiji plugin for 3D image registration with elastix', *Yenodo*.
- Toledo Acosta, Bertha Mayela. 2018. 'Multimodal image registration in 2D and 3D correlative microscopy', Rennes 1.
- Touboul, David, Felix Kollmer, Ewald Niehuis, Alain Brunelle, and Olivier Laprévotte. 2005. 'Improvement of biological time-of-flight-secondary ion mass spectrometry imaging with a bismuth cluster ion source', *Journal of the American Society for Mass Spectrometry*, 16: 1608-18.
- Ward, B. W., John A. Notte, and N. P. Economou. 2006. 'Helium ion microscope: A new tool for nanoscale microscopy and metrology', *Journal of Vacuum Science & Technology B: Microelectronics and Nanometer Structures Processing, Measurement, and Phenomena*, 24: 2871-74.
- Wentzensen, Nicolas, Ulf-Dietrich Braumann, Jens Eienkel, Lars-Christian Horn, Magnus von Knebel Doeberitz, Markus Löffler, and Jens-Peer Kuska. 2007. 'Combined serial section-based 3D reconstruction of cervical carcinoma invasion using H&E/p16INK4a/CD3 alternate staining', *Cytometry Part A*, 71A: 327-33.
- Yaniv, Ziv, Bradley C. Lowekamp, Hans J. Johnson, and Richard Beare. 2019. 'Correction to: SimpleITK Image-Analysis Notebooks: a Collaborative Environment for Education and Reproducible Research', *Journal of Digital Imaging*, 32: 1118-18.

Zitová, Barbara, and Jan Flusser. 2003. 'Image registration methods: a survey', *Image and Vision Computing*, 21: 977-1000.

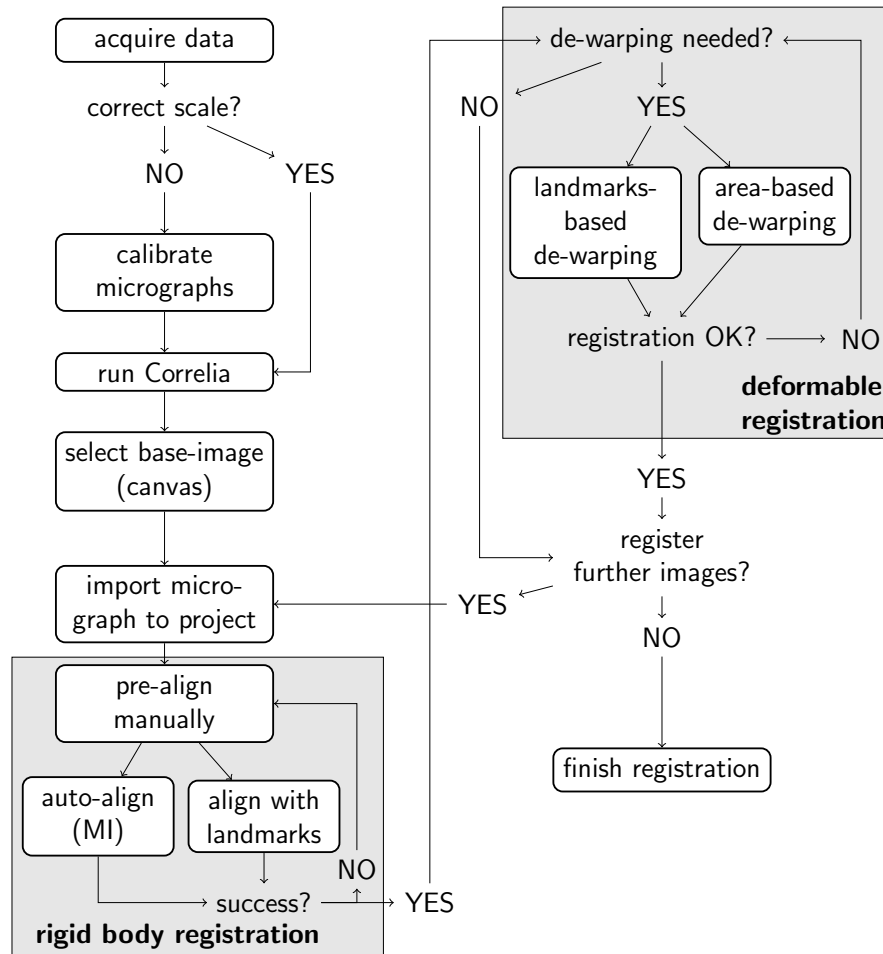


Figure 1: Workflow for the registration of correlative micrographs using *Correlia*.

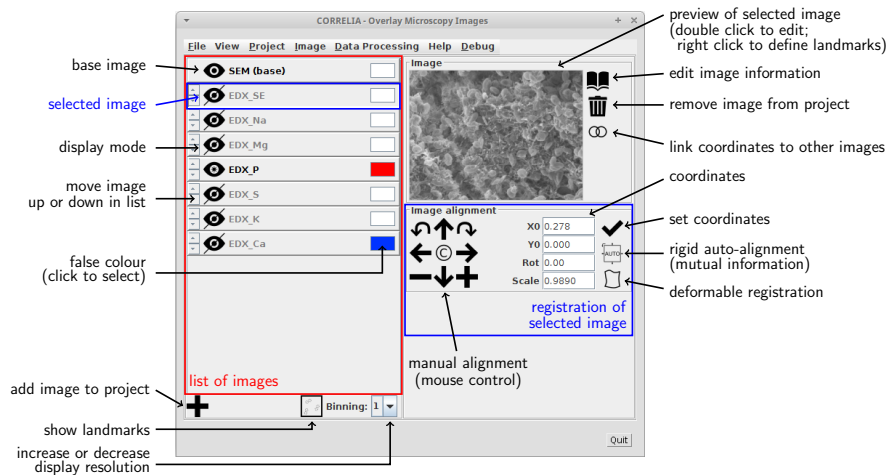


Figure 2: *Correlia*'s graphical user interface.

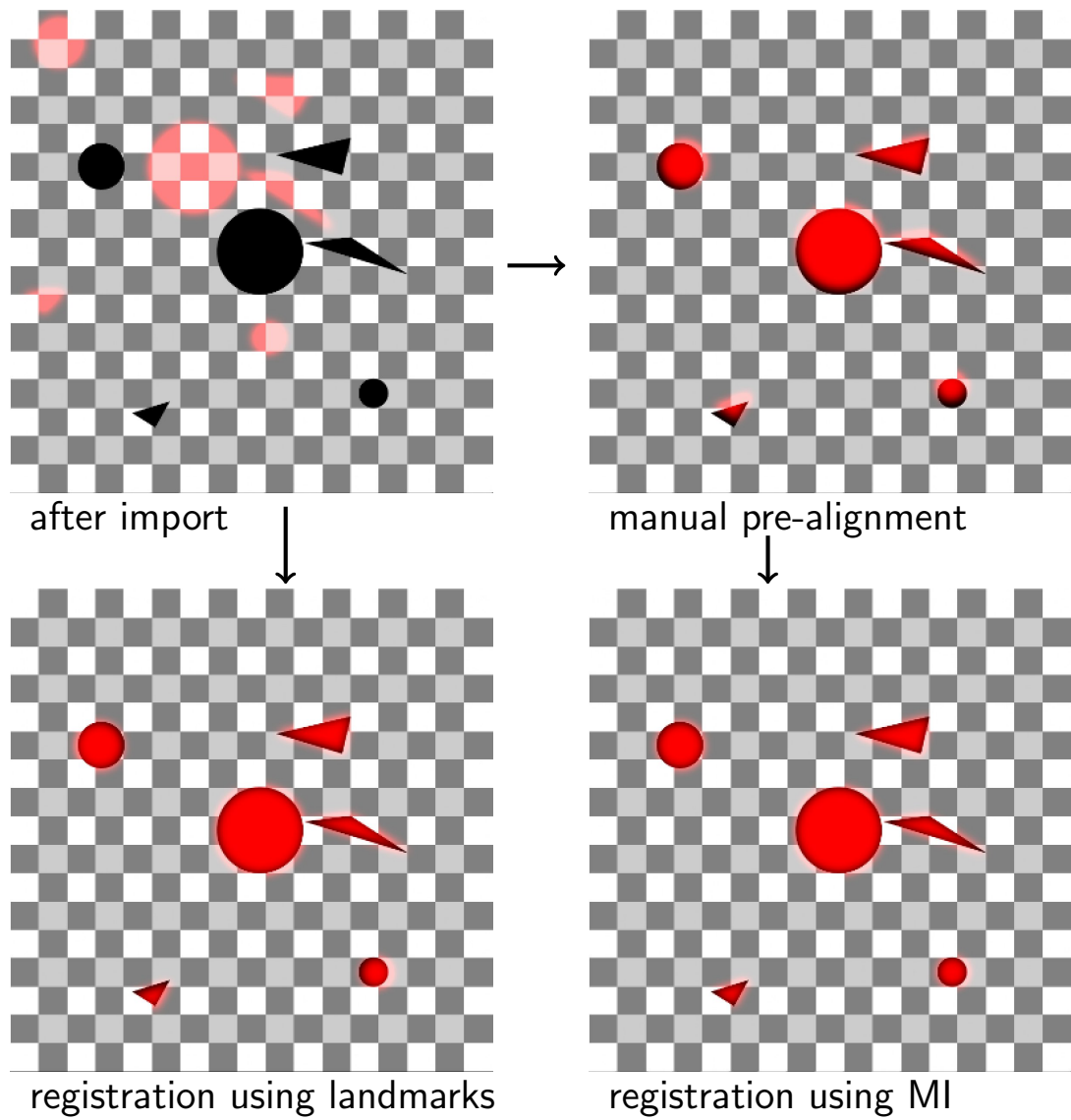
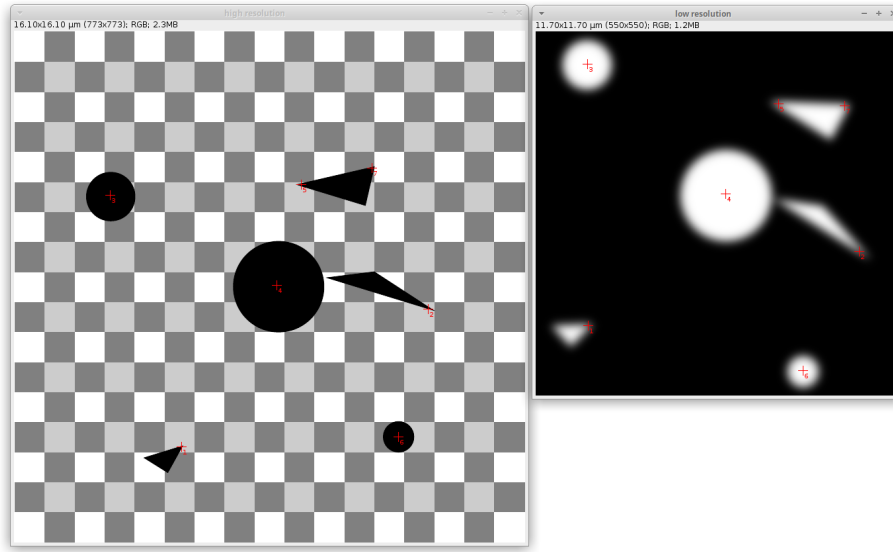
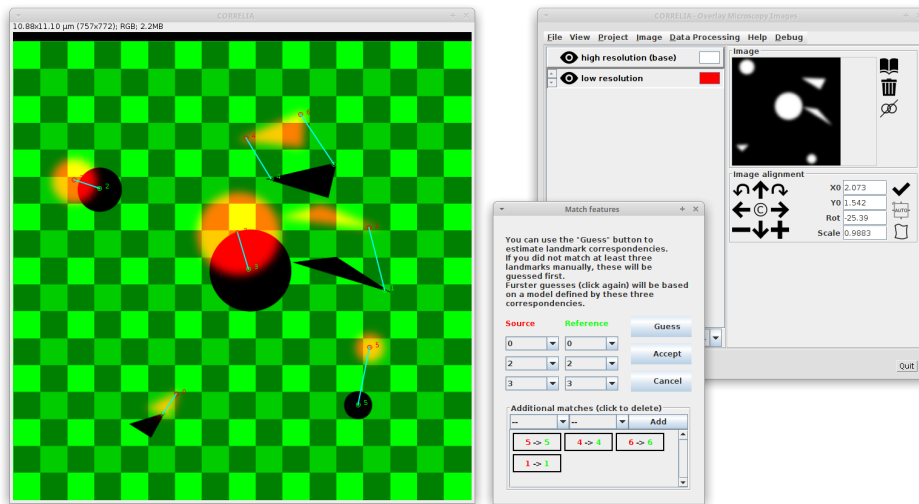


Figure 3: Illustration of the two possible ways for rigid body registration in Correlia. The moving image only contains some geometrical objects (red) which are supposed to align with the black objects on the chess board (target image). On the one hand corresponding landmarks can be defined in both, moving image and target which will be matched. On the other hand automatic registration using a mutual information approach is possible after a manual pre-alignment.



(A) definition of landmarks



(B) matching of corresponding landmarks

Figure 4: Rigid body registration using landmarks. A) At least three landmarks are defined in in moving image and target. B) Afterwards, corresponding features have to be matched. In the Match Features dialogue the user can either set the correspondences manually or ask the software to guess. The feature correspondences are then displayed with light blue lines in the viewer. The user acceptance of the correspondences will calculate the coordinates x and y as well as rotation and scale that will register the moving image onto the target.

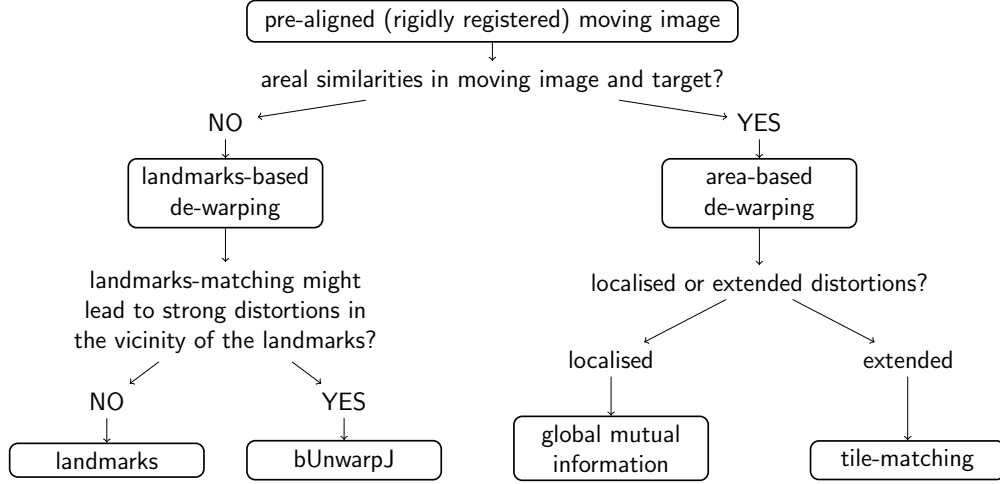


Figure 5: Rigid body registration cannot lead to a proper image alignment if distortions are present in the moving image. However, this can still be achieved by subsequently applying one or more of the deformable registration algorithms implemented in *Correlia* to de-warp the moving image. This flow chart shall help to select the most suitable one for the given registration problem.

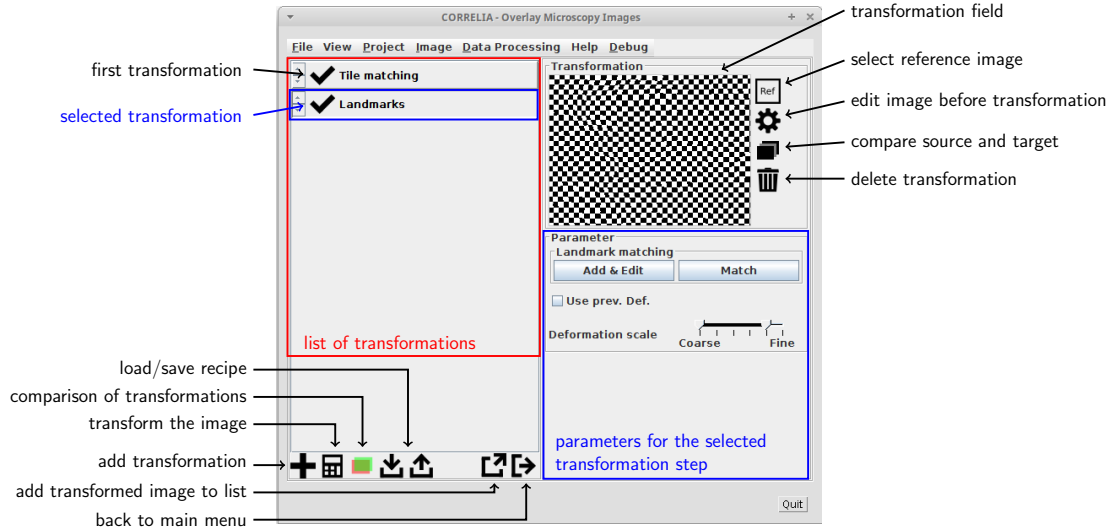


Figure 6: *Correlia*'s graphical user interface for deformable image registration. Several transformation steps can be cascaded and are listed on the left (here: tile matching followed by landmarks). The chess-board image on the right displays the transformation field. The parameters for the selected transformation are shown below.

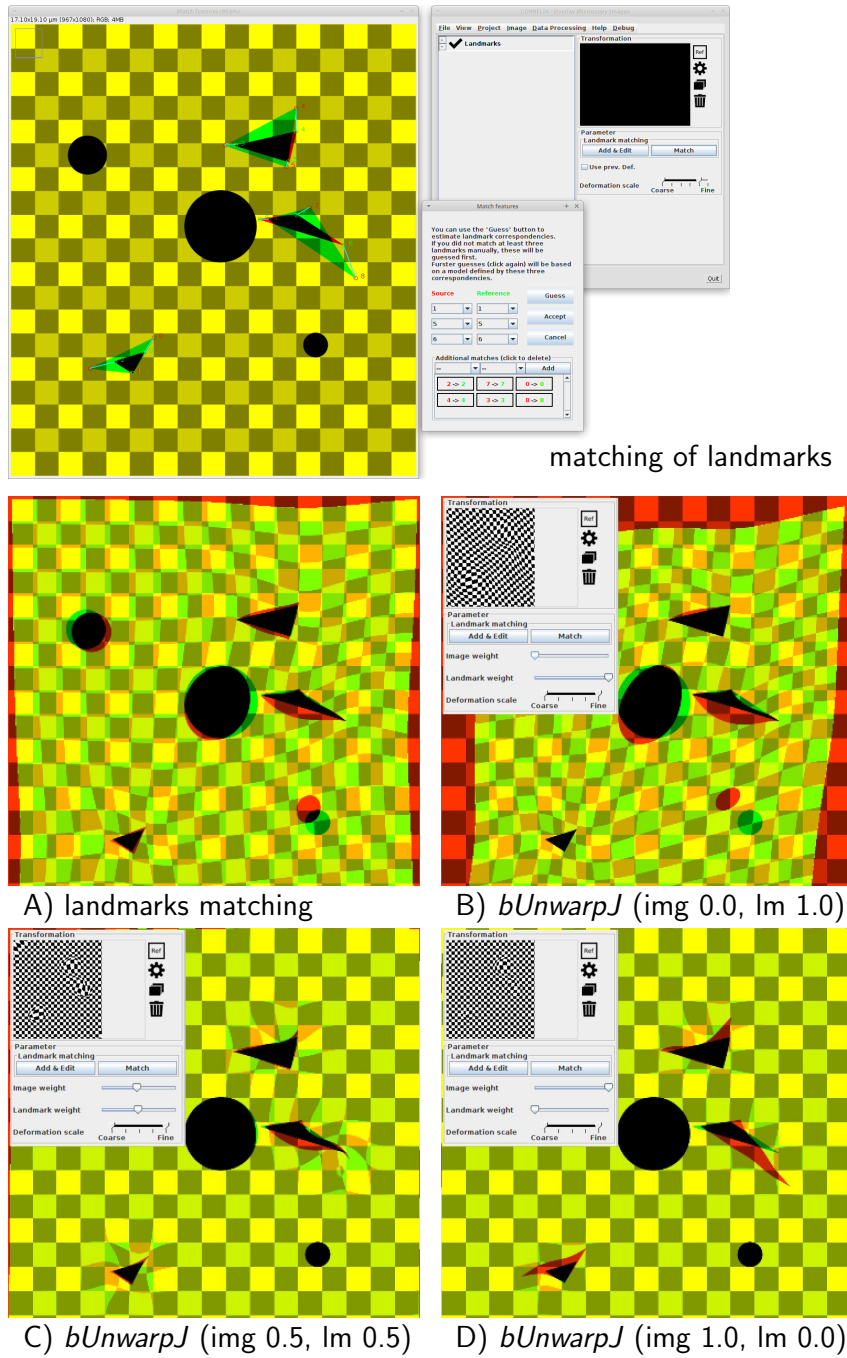


Figure 7: If a distorted moving image contains feature-points that have correspondences in the target, landmarks can be defined in both and forced to align. *Correlia* supports pure landmark-matching but also uses the external plug-in *bUnwarpJ*. The latter offers the possibility to transform the moving image in different ways by putting certain weight on image content (img) and landmarks (lm).

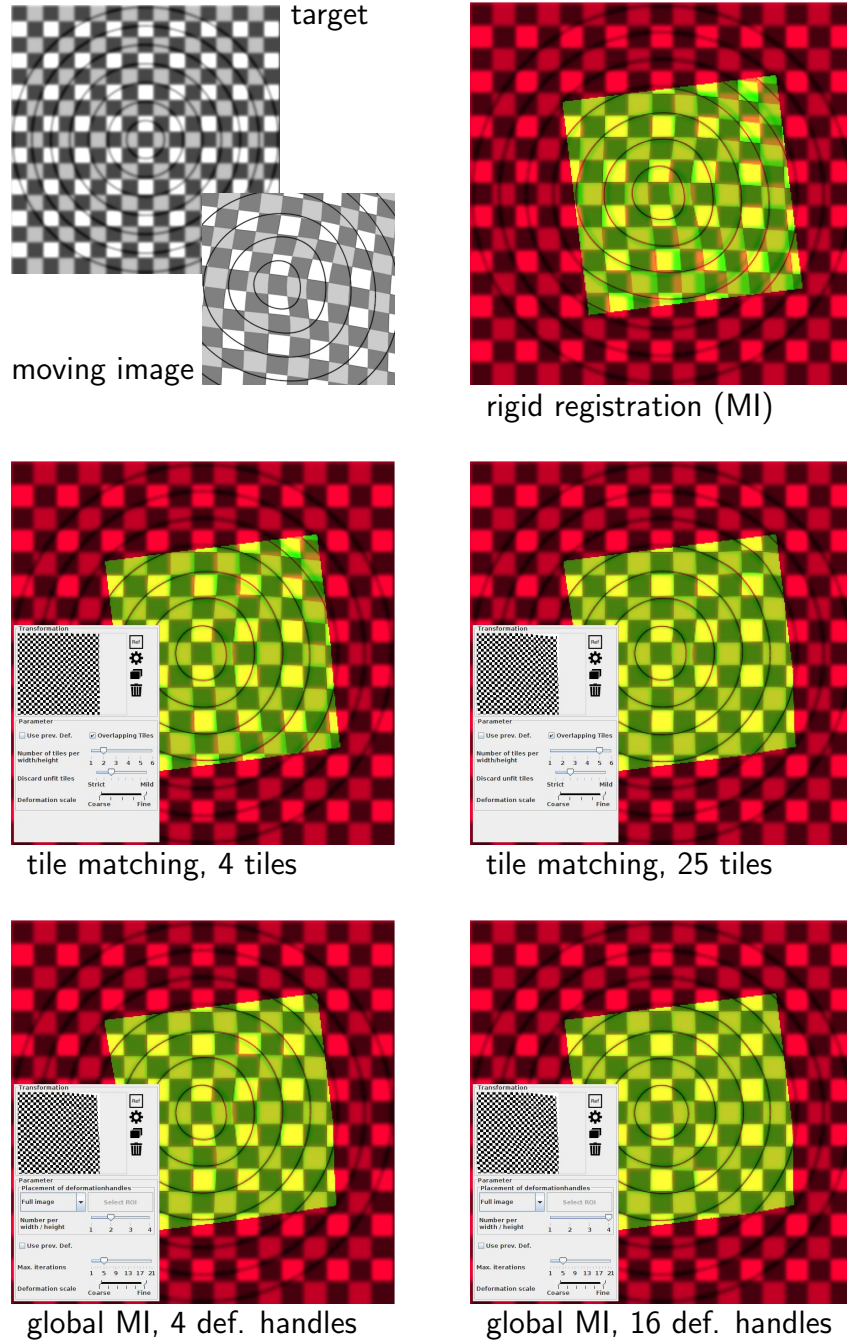


Figure 8: Registration of a moving image with artificial areal distortions onto a non-distorted but Gaussian-blurred target. After rigid pre-registration the moving image was warped to align with the target. For that tile matching with 4 and 25 tiles as well as global mutual information using 4 and 16 deformation handles were used, respectively.

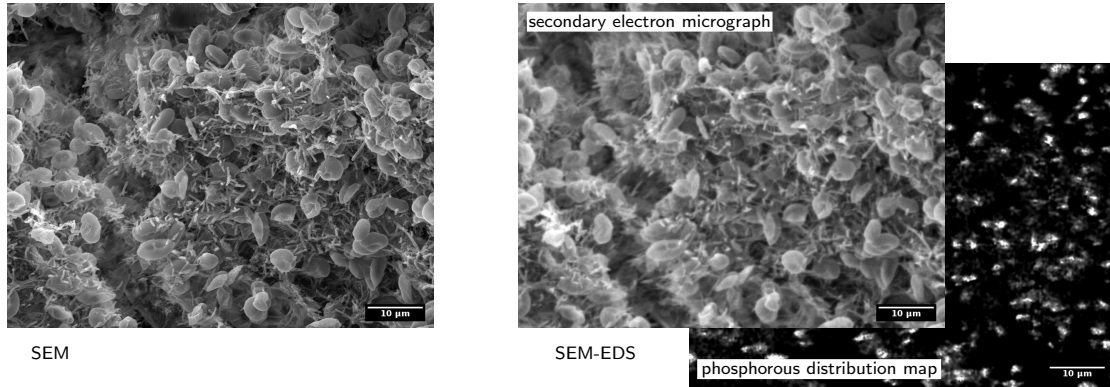


Figure 9: Investigation of the distribution of phosphorous in a biofilm of *Chlorella sp.* microalgae. A scanning electron micrograph (SEM, left) shall be overlaid with energy-dispersive X-ray spectroscopy maps (SEM-EDS, right). For that the secondary electron micrograph of the SEM-EDS data has to be registered onto the SEM image. Once that is the done the same transformation can be applied to the phosphorous map which then will be registered as well.

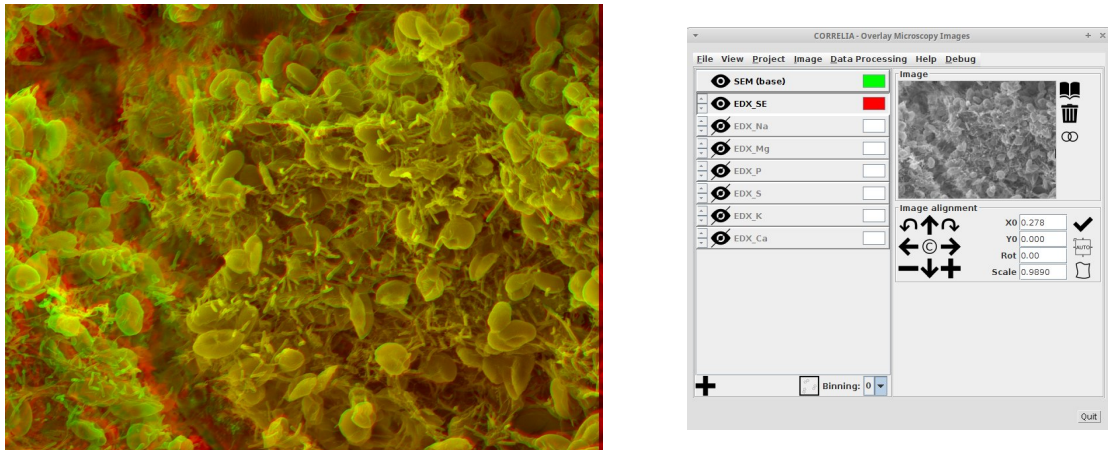


Figure 10, Rigid registration: Difference representation of the result of automatic rigid registration of SEM-EDS-SE (red) onto the SEM image (green) taken on the algal biofilm displayed in Fig. 9. Whilst the right side of the overlay aligns well, distortions along the crack on the left of the overlay are obvious and call for further deformable transformation.



Figure 11, Deformable registration 1 (tile matching): Difference image of SEM (green) overlaid with SEM-EDS secondary electron micrograph (red) of the algal biofilm shown in Fig. 9 and 10 after the first deformable registration using the tile matching approach. The tile-matching was carried out with 6×6 tiles distributed over the source micrograph allowing for full deformation scale. In particular on the left side of the image a significant improvement of the registration was achieved.

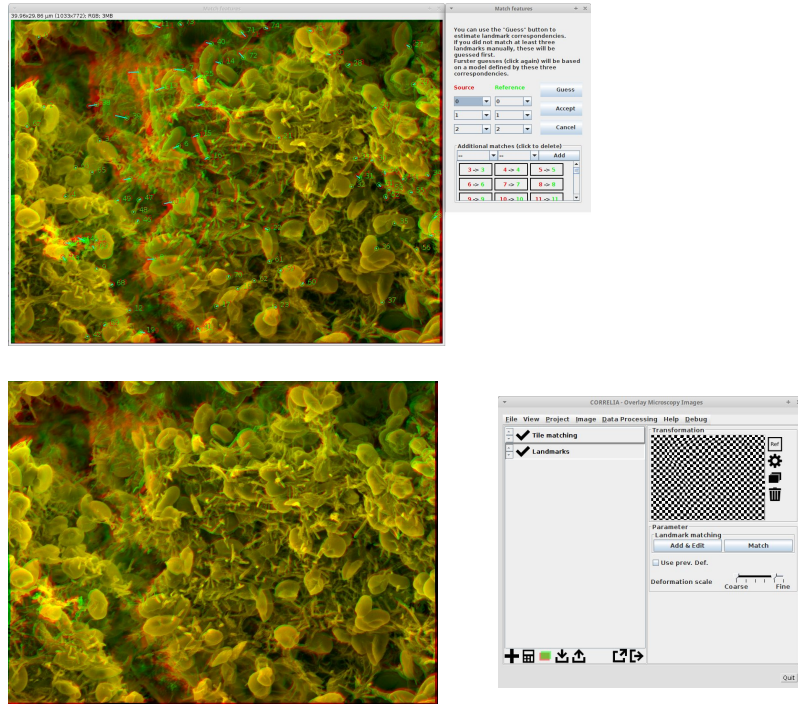


Figure 12, Deformable registration 2 (landmarks matching): After rigid pre-alignment (Fig. 10) and a deformable registration step (tile matching, Fig. 11) a final deformable registration step using landmarks matching is employed to properly register SEM image (green) and SEM-EDS secondary electron micrograph (red) acquired on a *Chlorella sp.* biofilm. In the upper part of the figure the distribution of landmarks in both micrographs is shown. The lower part shows the registration result after matching them.

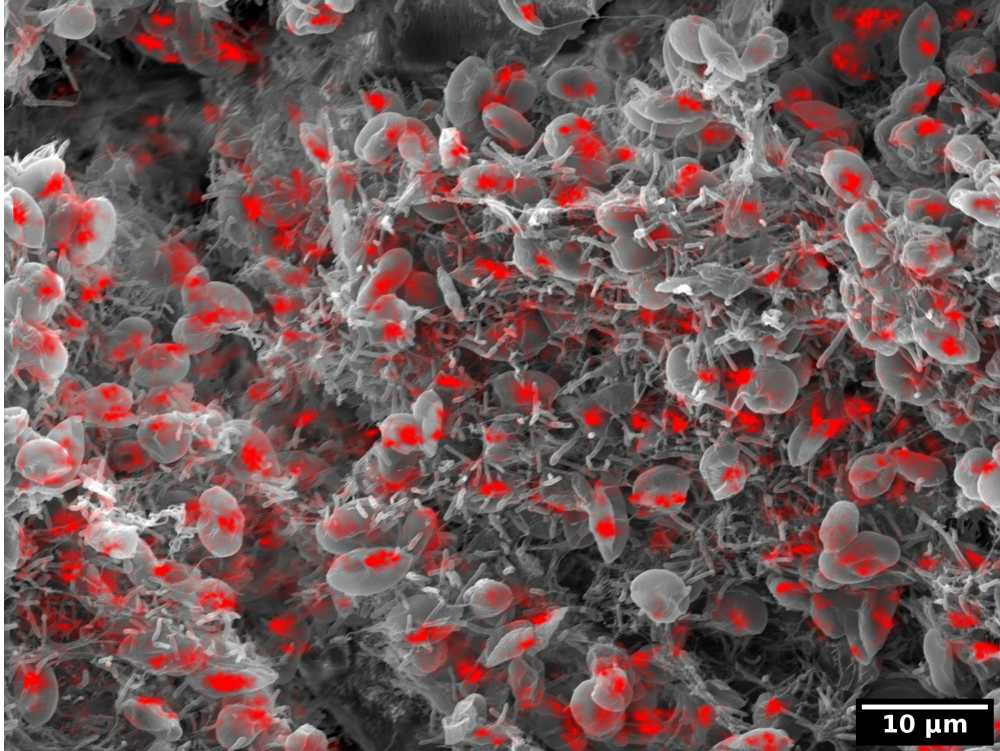


Figure 13: Application of the transformation model obtained by deformable registration of the SEM-EDS secondary electron micrograph onto the SEM image measured on an algal biofilm of *Chlorella sp.* microalgae (Fig. 12) to SEM-EDS phosphorous distribution map (shown in red). This overlay with the SEM image shows that the microalgae store excess phosphorous inside the cells rather than in the matrix of exopolymeric substances in the biofilm.

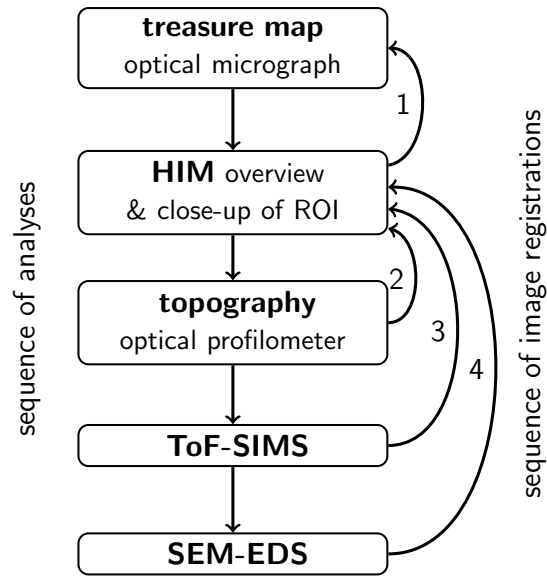


Figure 14: Workflow illustrating the sequence of microscopic analyses of the soil sample and at the same time the sequence of image registration applied to the so obtained correlative microscopy data.

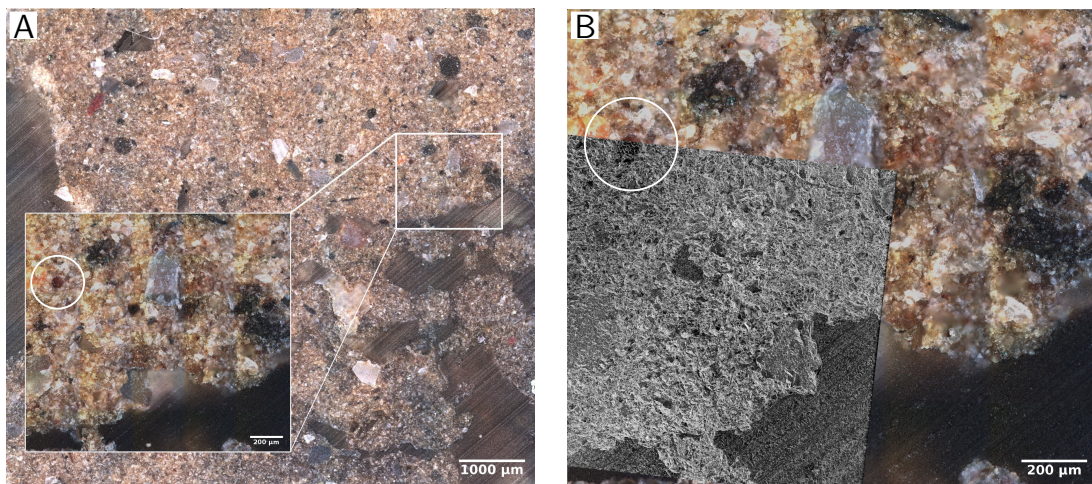


Figure 15: Treasure maps acquired on the soil sample. A) Stitched bright field image of the sample with the region of interest indicated and magnified. A root is found and encircled in white. B) The bright-field image of the region of interest serving as canvas (base image) for the *Correlia* project is overlaid with a helium-ion micrograph.

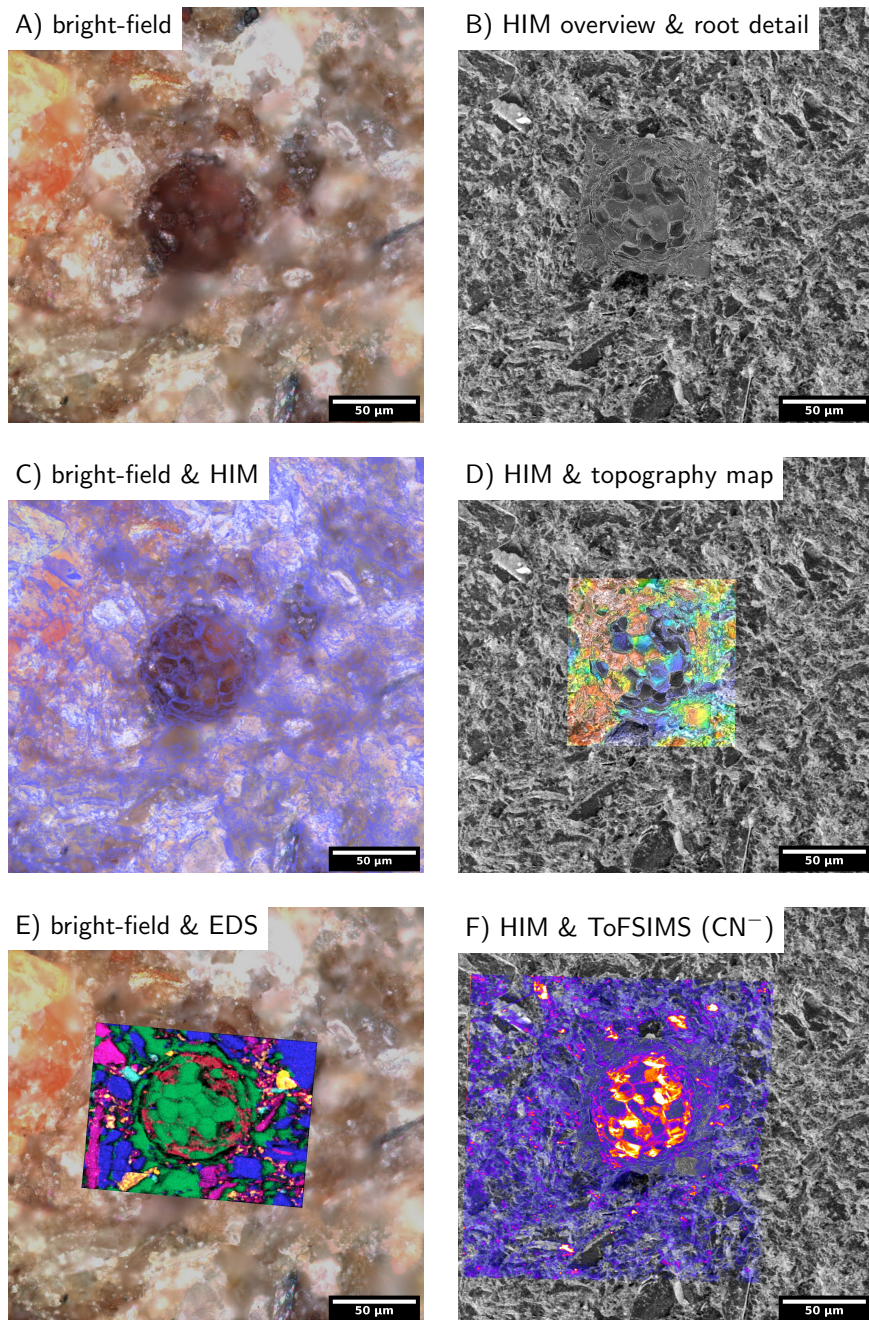


Figure 16: Organisation and visualisation of different modalities: A) Bright-field micrograph of the root found in the soil sample acquired with the optical profilometer. B) The same field-of-view imaged with the helium-ion microscope. A close-up of the root was taken at higher resolution and registered (rigid) onto the overview image. C) Overlay of bright-field image and HIM (false coloured in blue). D) Topography map measured with the optical profilometer using a 100x air-objective registered onto the

HIM image. The difference in height, from dark blue to red, amounts to 17 microns. E) Composite of chemical maps acquired by SEM-EDX registered onto the bright-field micrograph. F) Intensity map of CN⁻ ions measured by ToF-SIMS deformed and registered onto the helium ion micrograph.

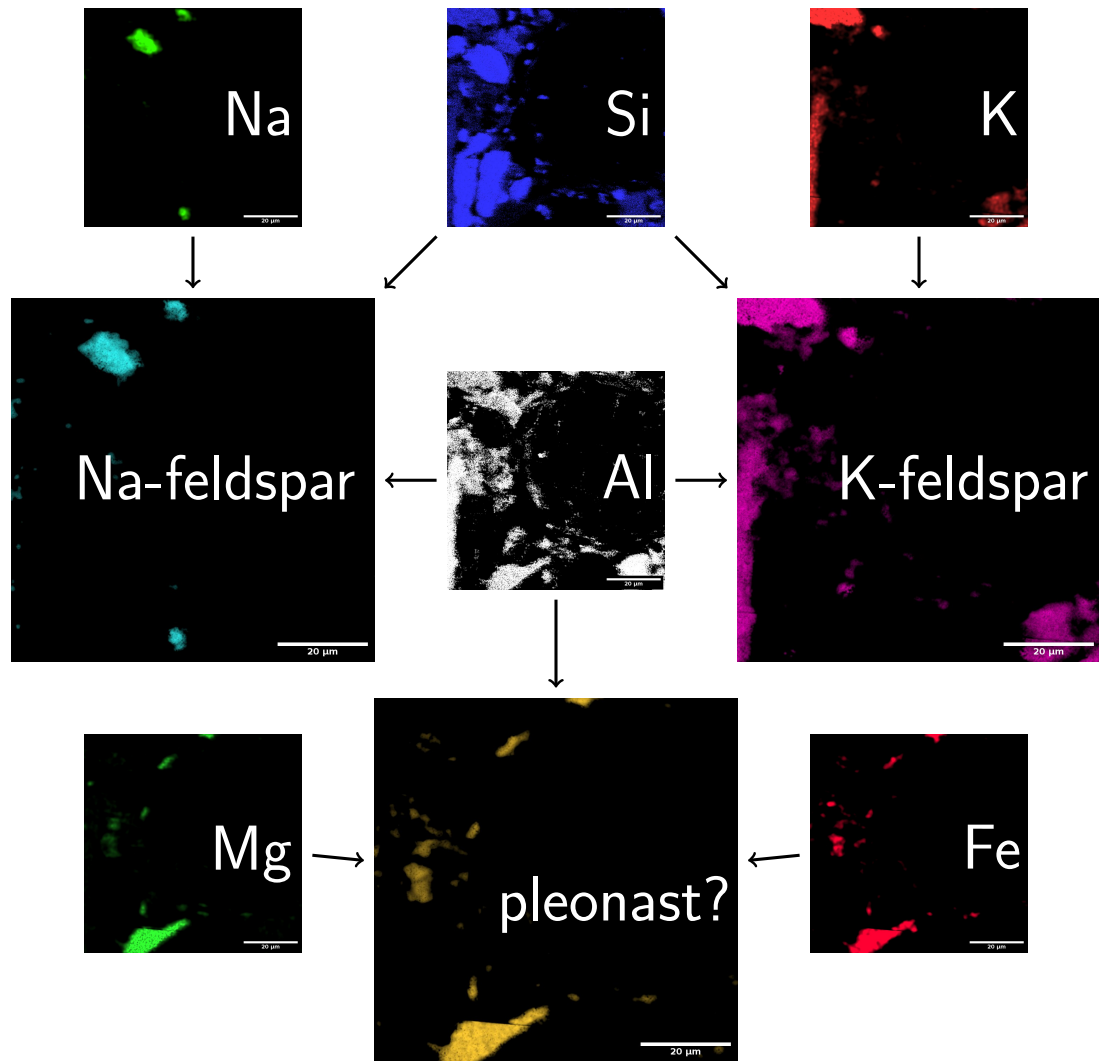


Figure 17: Correlation of SEM-EDS maps: If element distribution maps measured by SEM-EDS are pixelwise multiplied additional chemical information can be gained. Here for instance, different aluminium silicates can be grouped into different types of feldspar with aid of the Na and K maps. Furthermore the correlation of Mg, Al and Fe maps hints to the presence of the mineral pleonast in the sample. The composite image of the gained mineralogical maps is shown in Fig. 18.

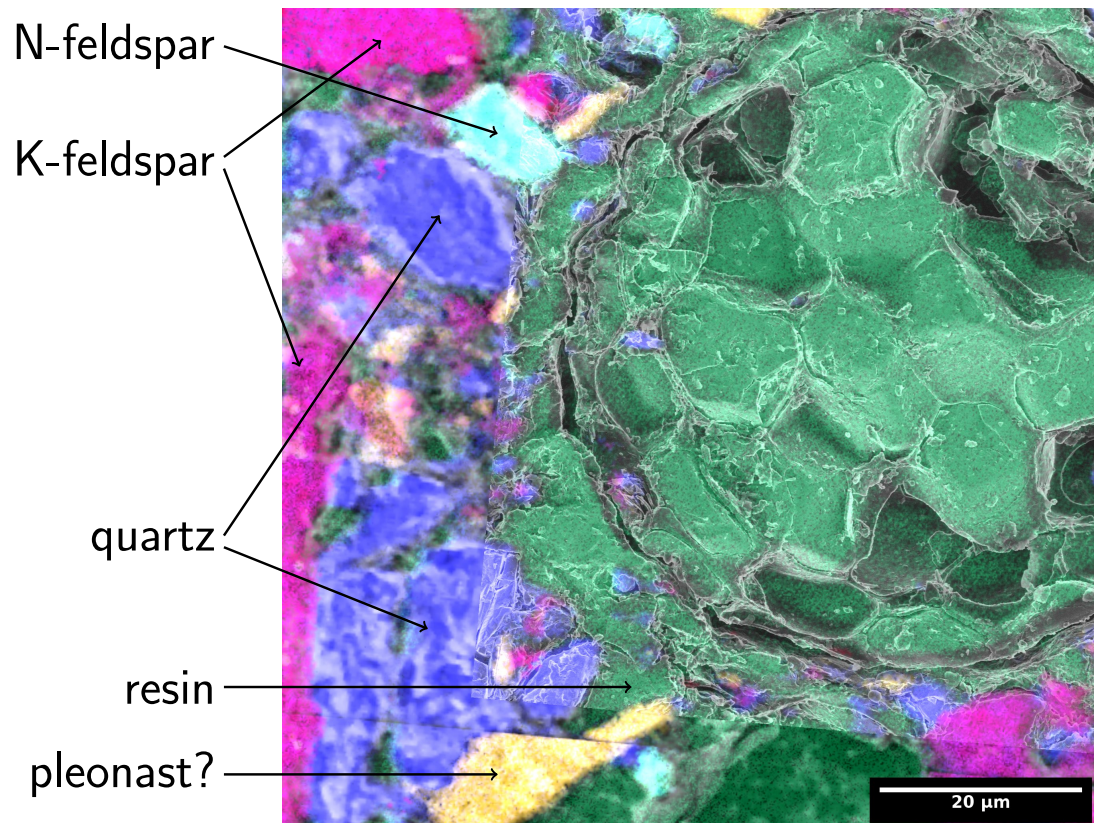


Figure 18: Overlay of the helium-ion micrograph and mineralogical maps gained from the correlation of SEM-EDS chemical maps. Plant-cells in the root and pores are filled with resin (green, measured as carbon distribution map by SEM-EDS). The minerals in the vicinity of the root are quartz and different feldspar minerals.

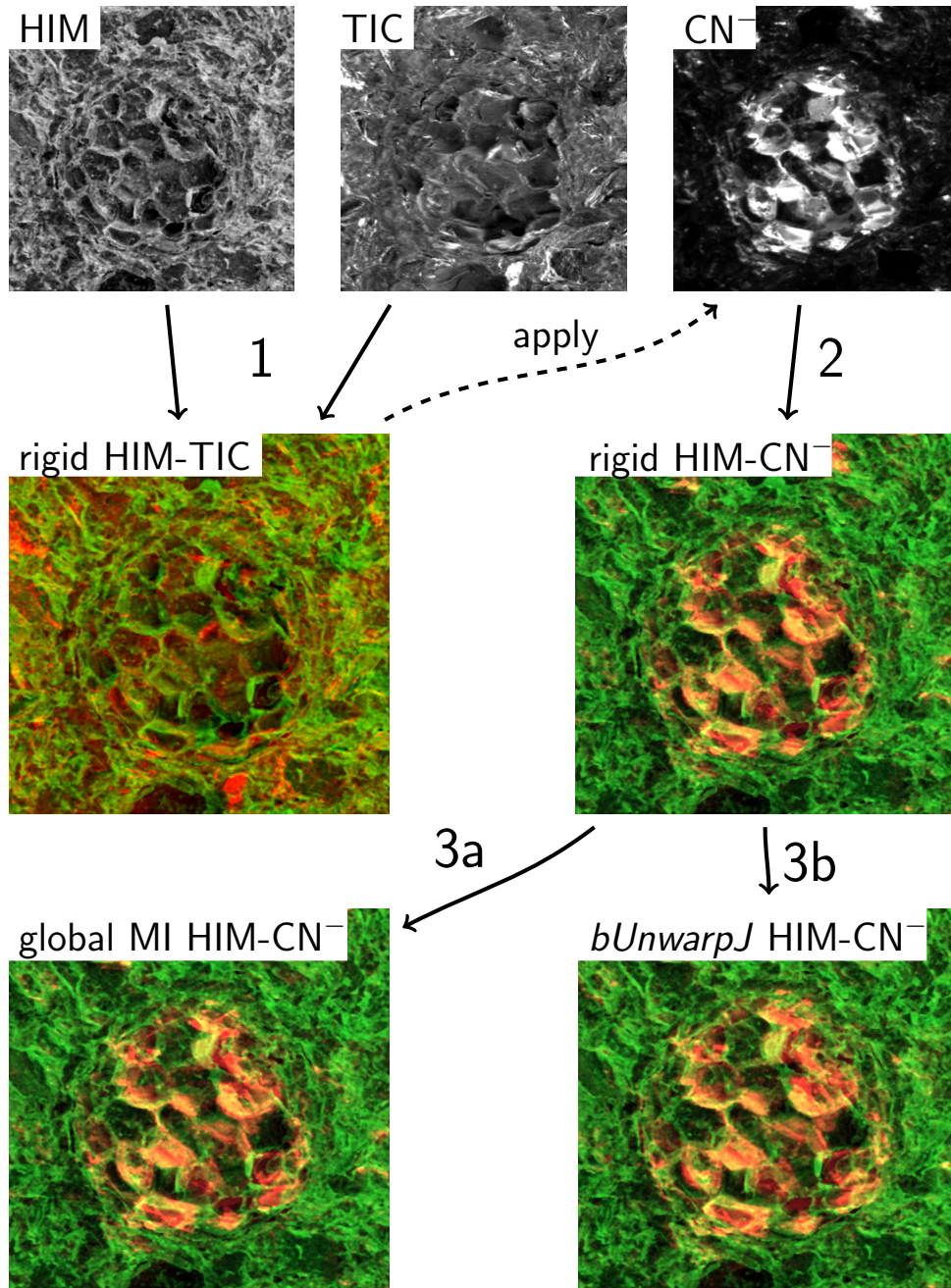


Figure 19: Registration of ToF-SIMS data onto HIM: 1) The ion count (TIC) obtained from ToF-SIMS is very similar to the helium-ion micrograph. After rigid registration the difference image with HIM in green and ToF-SIMS in red shows a good correlation. 2) Applying this transformation model to the CN^- ion distribution map. Deformable registration can locally improve the quality of the registration as shown by the results of global mutual information (3a) and *bUnwarpJ* (3b).